*Astronomy & Astrophysics* manuscript no. Venturi-accepted
October 30, 2012
© ESO 2012

arXiv:1210.7617v1 [astro-ph.CO] 29 Oct 2012

# Low frequency follow up of radio halos and relics in the GMRT Radio Halo Cluster Survey

T. Venturi[1], S. Giacintucci[2,3], D. Dallacasa[4], R. Cassano[1], G. Brunetti[1], G. Macario[5], R. Athreya[6]

[1] INAF – Istituto di Radioastronomia, via Gobetti 101, I-40129, Bologna, Italy
[2] Department of Astronomy, University of Maryland, College Park, MD 20742-2421
[3] Joint Space-Science Institute, University of Maryland, College Park, MD, 20742-2421, USA
[4] Dipartimento di Astronomia, Università di Bologna, via Ranzani 1, I-40126 Bologna, Italy
[5] Laboratoire Lagrange, UMR7293, Université de Nice Sophia-Antipolis, CNRS, Observatoire de la Côte d'Azur, 06300 Nice, France
[6] Indian Institute of Science Education and Research (IISER), Pune, India

Received 00 - 00 - 0000; accepted 00 - 00 - 0000

## ABSTRACT

*Aims.* To gain futher insight on the origin of diffuse radio sources in galaxy clusters and their connection with cluster merger processes, we performed GMRT low frequency observations of the radio halos, relics and new candidates belonging to the GMRT Radio Halo Cluster Sample first observed at 610 MHz. Our main aim was to investigate their observational properties and integrated spectrum at frequencies below 610 MHz.
*Methods.* High sensitivity imaging was performed using the GMRT at 325 MHz and 240 MHz. The properties of the diffuse emission in each cluster were compared to our 610 MHz images and/or literature information available at other frequencies, in order to derive the integrated spectra over a wide frequency range.
*Results.* Cluster radio halos form a composite class in terms of spectral properties. Beyond the classical radio halos, whose spectral index $\alpha$ is in the range $\sim 1.2 \div 1.3$ ($S \propto \nu^{-\alpha}$), we found sources with $\alpha \sim 1.6 \div 1.9$. This result supports the idea that the spectra of the radiating particles in radio halos is not universal, and that inefficient mechanisms of particle acceleration are responsible for their origin. We also found a variety of brightness distributions, i.e. centrally peaked as well as clumpy halos. Even though the thermal and relativistic plasma tend to occupy the same cluster volume, in some cases a positional shift between the radio and X–ray peaks of emission is evident. Our observations also revealed the existence of diffuse cluster sources which cannot be easily classified either as halos or relics. New candidate relics were found in A 1300 and in A 1682, and in some clusters "bridges" of radio emission have been detected, connecting the relic and radio halo emission. Finally, combining our new data with literature information, we derived the $\mathrm{LogL_X}$–$\mathrm{LogP_{325\ MHz}}$ correlation for radio halos, and investigated the possible trend of the spectral index of radio halos with the temperature of the intracluster medium.

**Key words.** radio continuum: galaxies - galaxies: clusters: general - galaxies: clusters: individual: A 209, A 781, A 1300, A 1682, A 1758N, A 2744, Z 2661, RXCJ 1314.5–2515

## 1. Introduction

Our understanding of the interplay between the thermal and non–thermal components in clusters of galaxies, as well as their link to the processes leading to the formation of massive clusters in the hierarchical scenario, has considerably improved thanks to the high sensitivity of radio interferometers such as the Very Large Array (VLA) and the Giant Metrewave Radio Telescope (GMRT), and to the advent of the Chandra and XMM-Newton X–ray observatories.

Non–thermal radio emission in galaxy clusters may take the form of radio halos and relics, diffuse and extended sources (up and above the Mpc) of low surface brightness (of the order of the $\mu$Jy arcsec$^{-2}$) with no obvious optical counterpart, which have so far been found in $\sim$ 40–50 clusters. They prove the existence of relativistic particles (with Lorentz factor $\gamma \gg 1000$) and large scale $\mu$G magnetic fields. Their power–law radio spectrum, with typical spectral index $\alpha \sim 1.2 - 1.3$[1] is the signature of a synchrotron origin (see Ferrari et al. 2008, Venturi 2011 and Feretti et al. 2012 for recent observational reviews). Beyond the similar observational properties, halos and relics differ in the location within the cluster and in the polarization properties. Radio halos are centrally located, with a rather regular shape usually coincident with the distribution of the intracluster medium (ICM) and are unpolarized (exception made for MACS J0717.5+3745, Bonafede et al. 2009), suggesting that the radio emission comes from a region co–spatial with the X–ray emitting gas. On the other hand, relics are found in peripheral cluster regions and usually exhibit an elongated structure and high fractional polarization (e.g., Clarke & Enßlin 2006, van Weeren et al. 2010), suggesting that they are located in external regions of the clusters, or seen in projection on the cluster centre.

The longstanding key question concerns the origin of halos and relics, since the radiative life–time of the radiating electrons is much shorter than the diffusion time necessary to cover the cluster scale volumes, therefore some form of in–situ particle acceleration is needed to account for their existence (Jaffe 1977; see also Cassano 2009 and Brunetti 2011 for recent reviews).

---

[1] $S_\nu \propto \nu^{-\alpha}$, where $S_\nu$ is the flux density at the frequency $\nu$.

All models proposed to explain the origin of relic sources invoke the presence of a shock in the thermal gas, possibly induced by dynamical activity within the cluster (Enßlin et al. 1998; Enßlin & Gopal–Kishna 2001; Hoeft & Brüggen 2007). So far a spatial connection between a X–ray shock, or candidate, and cluster–scale radio emission in the form of a distinct radio relic, or an edge in the radio halo structure, has been reported only for a handful of clusters, i.e. the Bullet cluster (Markevitch et al. 2002); A 520 (Markevitch et al. 2005); A 754 (Macario et al. 2011a); A 3667 (Finoguenov et al. 2010; A 521 (Giacintucci et al. 2008 and Bourdin et al. 2012); CIZA J 2242.8+5301 (Ogrean et al. 2012); RXCJ 1314.5–2515 (Mazzotta et al. 2011). A census of the relics studied so far is given in van Weeren et al. 2011; a review of our knowledge of shocks and of the related radio emission has been recently given in Markevitch (2010).

The origin of giant radio halos is more debated. A popular scenario, the so called "re–acceleration model" (a modern elaboration of the class of the "in–situ" acceleration scenario, first proposed by Jaffe 1977 and Roland 1981, and quantitatively developed by Schlickeiser et al. 1987), assumes that relativistic electrons are re–accelerated in the ICM by MHD turbulence injected in the cluster volume by merger events (Brunetti et al. 2001; Petrosian 2001, Fujita et al. 2003). This scenario is motivated by the observed connection between radio halos and cluster mergers and by considerations on the spectra of radio halos, which appear to favour mechanisms which are not very efficient in the acceleration of the emitting particles (see Brunetti 2011 for a recent overview). Alternative models assume that the relativistic electrons are secondary products of the collisions between the intergalactic cosmic rays and the thermal protons in the ICM (the so–called "secondary models", see Dennison 1980, Blasi & Colafrancesco 1999, Pfrommer & Enßlin 2004, Keshet & Loeb 2010). These models are based on the argument of cosmic ray confinement in the intracluster medium, and on the fact that the production of secondary electrons, at least to some extent, is unavoidable. More recently, turbulent re–acceleration of relativistic protons and secondary particles has also been investigated (Brunetti & Blasi 2005, Brunetti & Lazarian 2011).

The GMRT Radio Halo Survey (Venturi et al. 2007 and 2008, V07 and V08 respectively) has provided a first insight into the statistical properties of radio halos. It has been shown that radio halos are a transient phenomenon, being hosted only in ∼30% of massive clusters (Cassano et al. 2006 and 2008; Cassano 2009) undergoing major mergers, as quantitatively derived from the analysis of the X–ray emission. Conversely, to date no halos have been detected in dynamically relaxed clusters (Cassano et al. 2010). These results support the importance of turbulence in re–accelerating and confining the emitting particles in cluster mergers (Brunetti et al. 2009, Enßlin et al. 2011).

Turbulent re–acceleration models further predict the existence of a composite population of radio halos, with spectral index steeper than studied so far at centimeter wavelentghs. It is now clear that such sources exist: the radio halo in A 521, with a spectral slope $\alpha \sim 1.9$, is considered the prototype of these "ultra–steep spectrum radio halos" (USSRH) (Brunetti et al. 2008 and Dallacasa et al. 2009). The current status of our knowledge of the diffuse sources in galaxy clusters can be found in the books of recent conference proceedings on this topic (Ferrari et al. 2011, Dwarakanath et al. 2011).

The largest majority of radio halos and relics have been detected and imaged only at 1.4 GHz (i.e. Bacchi et al. 2003, Govoni et al. 2001 and 2004, Giovannini et al. 2009), and interferometric high sensitivity observations at frequencies $\nu \leq 325$ MHz are available only in a handful of cases. As a result, our knowledge of the properties of halos and relics and of their spectra at frequencies below $\nu \sim 325$ MHz is still poor and incomplete. To start filling this gap, we performed high sensitivity low frequency follow–up observations of all the cluster sources (radio halos and relics) and candidate diffuse emission detected with the GMRT at 610 MHz, as well as the known radio halos in the GMRT cluster sample still lacking information at frequencies below 1.4 GHz (V07 and V08). The clusters were surveyed at 325 MHz, and some of them were followed up at 240 MHz as well.

In this paper we report on the results of our 325 MHz and 240 MHz GMRT observations. The paper is organised as follows: in Section 2 we present the radio observations and data reduction; in Section 3 we present the 325 MHz and 240 MHz radio analysis of the radio halos and diffuse sources; in Section 4 we discuss our results. Conclusions are given in Section 5.

We adopt the ΛCDM cosmology, with $H_0$=70 km s$^{-1}$ Mpc$^{-1}$, $\Omega_m = 0.3$ and $\Omega_\Lambda = 0.7$.

## 2. Observations and data reduction

### 2.1. The cluster sample

From the GMRT radio halo cluster sample (V07 and V08) we selected all clusters with a diffuse source, either in the form of radio halo or relics, and those with "suspect" diffuse emission, for a low frequency follow–up. Table 1 provides the list of all clusters in our project. The legend to Column 5 is: GRH=giant radio halo[2]; RH=radio halo; Rel=relic.

Four clusters in Table 1 have been published in dedicated works: A 521 (Giacintucci et al. 2008 and Brunetti et al. 2008), A 697 (Macario et al. 2010), A 781 (Venturi et al. 2011a), RXCJ 2003.5–2323 (Giacintucci et al. 2009). In this paper we present the remaining clusters, and we incorporate all the clusters in Table 1 in the discussion.

### 2.2. Data reduction and imaging

All clusters except A 1682 were observed at 325 MHz for a total of approximately 8 hours, using both the upper and lower side band (USB and LSB, respectively), left and right polarization, for a total observing bandwidth of 32 MHz. The data were recorded in spectral–line mode with 128 channels/band, leading to a spectral resolution of 125 kHz/channel. A 1682 was observed for ∼ 6 hours in dual band at 240/610 MHz as part of a 610 MHz re–observation (610 MHz data presented in V08), with a 240 MHz bandwidth of 8 MHz spread over 64 spectral channels. Night observing was carried out for all sources, to minimize the effects of ionosphere and radio frequency interference (RFI). Table 2 reports the observational details.

---

[2] Linear size ≥ 1 Mpc as defined in CB05, with $H_0$=50 km s$^{-1}$ Mpc$^{-1}$. This size corresponds to $\gtrsim$700 kpc with the cosmology assumed in this paper.

The USB and LSB datasets were calibrated and reduced individually using the NRAO Astronomical Image Processing System (AIPS) package. Strong RFI affected each observation, and in some cases only one portion of the band was used to produce the final images (see individual comments in the next section and notes to Table 2). For this reason, beyond the standard flagging of bad baselines, antennas and time ranges, we carried out a very accurate inspection of each dataset in order to identify and remove those data affected by RFI. In all cases the bandpass calibration was performed using the flux density calibrator. The calibration solutions were applied to the data by running the AIPS task FLGIT, which subtracts a continuum from the channels in the u–v plane, determined on the basis of the bandpass shape and using a specified set of channels. Those data whose residuals exceeded a chosen threshold were flagged.
Each dataset was then averaged to 6 channels of ∼2 MHz each. Given the large field of view of the GMRT, each step of the self–calibration cycle was carried out by means of the wide–field imaging technique to account for the non–planar nature of the sky. We used 25 facets covering a total field of view of $\sim 2.7^\circ \times 2.7^\circ$ . In those cases where both USB and LSB could be used, after a number of phase self–calibration cycles, the final USB and LSB datasets were further averaged from 6 channels to 1 single channel, and then combined together to produce the final images. Note that bandwidth smearing is relevant only at the edge of the wide field of view at 325 MHz and 240 MHz, and does not affect the central cluster regions presented and analysed in this paper.

Despite the massive editing required by the RFI in some cases, the quality of the images is generally good; the $1\sigma$ rms level is in the range 0.1–0.5 mJy beam$^{-1}$. The rms values reported in Table 2 were measured on the full resolution images. We estimate that the residual amplitude errors are of the order of$\lesssim$5%.
For all clusters we produced sets of final images, from the full GMRT resolution ($\sim 10''$ at 325 MHz, and $\sim 13''$ at 240 MHz) to tapered images with typical resolution of the order of $\sim 35'' - 40''$.

In order to properly image the diffuse cluster radio emission, it is necessary to subtract the contribution (to the flux and morphology) of the embedded discrete sources. Thanks to its configuration, which provides a simultanous good coverage of short and long spacings in the u–v plane, the GMRT is particularly suited to perform accurate source subtraction. Where necessary, we carefully subtracted the individual sources from the u–v data, and then produced images of the diffuse cluster sources from the subtracted dataset. In particular, point–like sources with peak flux density $\geq 5-6\sigma$ were subtracted from the diffuse emission in the u–v plane. For careful subtraction of the extended radio galaxies we made an image cutting the innermost regions of the u–v plane to avoid subtraction of any possible contribution from the diffuse cluster emission, and tapering the visibilities for best imaging of their extended emission. We then subtracted the clean components from the u–v data and finally imaged the source subtracted dataset. For each source (point–like and extended), we ensured consistency between the total flux density subtracted as clean components from the u–v data and the flux density measured in the full resolution image.
We are confident that any residual contribution of emission from extended sources to the flux and morphology of the diffuse cluster emission is neglibible. The contribution of faint embedded sources whose flux density is just below our threshold is also negligible: radio source counts show that the number of radio sources with mJy and sub–mJy flux density is of the order of ∼0.01 for a sky region with average largest angular size of $\sim 4-5'$, as is the case for the cluster sources presented in this paper (i.e. Bondi et al. 2007, Venturi et al. 2002 and references therein).

Considering the uncertainties in the source subtraction procedure, we associate a final error of 8% to the flux density of the diffuse sources.

## 3. Diffuse cluster sources at low frequency

For each cluster presented in this Section, Table 3 provides the position and flux density of the individual radio sources embedded in the diffuse emission, as measured on the full resolution images with the AIPS task JMFIT for unresolved sources and TVSTAT for extended sources. Table 4 summarizes the observational properties of the diffuse emission in each cluster (the morphological classification is given in Col. 2, the total flux density and linear size are reported in Col. 4 and 5 respectively) imaged after subtraction of the discrete radio galaxies listed in Table 3. The bottom part of Table 4 reports the information for the clusters presented in separate papers. In Table 5 we list the candidate diffuse cluster sources which still need to be confirmed.

### *3.1. Clusters with a giant radio halo*

### 3.1.1. A 209

A 209 (z=0.206) is a massive merging cluster with $L_{\rm X,[0.1-2.4~keV]} = 6.3 \times 10^{44}$ erg s$^{-1}$ (see V07 for a review of its properties). It hosts a giant radio halo, imaged with the GMRT at 610 MHz (V07) and with the VLA at 1.4 GHz (Giovannini et al. 2009, Giacintucci et al. 2013, hereinafter G12).
The 325 MHz data were affected by strong interference, which required massive data editing and prevented high quality imaging of the diffuse cluster emission: no individual source subtraction was performed for this cluster. Our images, presented in Fig. 1, are in agreement with those at 610 MHz, both in shape and extent (Fig. 2 in V07). The radio halo covers only the most luminous part of the X–ray emission, and is smaller than imaged at 1.4 GHz, most likely as consequence of the RFI removal editing, which forced us to drop many short spacings. The flux density of the radio halo, measured from the image shown in the right panel of Fig. 1 after subtraction of the flux density of the discrete radio sources S1 and S2 reported in Table 3 (Fig. 1 left), is $S_{\rm 325~MHz} = 74 \pm 6$ mJy. We consider this value, as well as the largest linear size measured from the right panel of Fig. 1 (Table 4), as lower limits. V07 reported a flux density $S_{\rm 610MHz} = 24.0 \pm 3.6$; Giovannini et al. (2009) report a value at 1.4 GHz of $S_{\rm 1.4GHz} = 16.9$ mJy, while a re–analysis of the archival VLA 1.4 GHz data performed in G12 led to a flux density estimate measurement $S_{\rm 1.4GHz} = 15.0 \pm 0.7$ mJy. Considering that the flux density of the radio halo at 610 MHz is most likely understimated (as discussed in

V08), and in the light of the limited quality of the 325 MHz data, we could not perform a spectral study for this cluster and did not include A 209 in the discussion carried out in Sect. 4.4.1.

#### 3.1.2. A 1758N

A 1758N (z=0.2782, Boschin et al. 2012; $L_{\rm X,[0.1-2.4KeV]}$ = $12.3 \times 10^{44}$ erg s$^{-1}$) is part of a well–known pair of two merging clusters, A 1758N and A 1758S, separated by ∼ 8′ in the plane of the sky and ∼ 2100 km s$^{-1}$ in the velocity space, both formed by two merging clusters (Ragozzine et al. 2012). A detailed Chandra and XMM–Newton X–ray study (David & Kempner 2004) reveals that both clusters are characterised by very complex X–ray morphology, with several clumps of emission, as commonly found in cases of ongoing cluster merging activity. A 1758N shows more extreme X–ray properties, with higher X–ray luminosity and temperature compared to A 1758S. Its total mass is ∼ $2{-}3{\times}10^{15}$M$_\odot$, and a new optical analysis confirms that it is a recent merger (Boschin et al. 2012, Ragozzine et al. 2012). A 1758N is also much more interesting in the radio band, with a well–known central narrow angle tail radio galaxy (O'Dea & Owen 1985) and diffuse central emission visible both on the Northern VLA Sky Survey (NVSS) and on the WEsterbork Northern Sky Survey (WENSS), as reported in Kempner & Sarazin (2001). VLA observations at 1.4 GHz were recently presented in Giovannini et al. (2009) and re–analysed in G12.

The images of A 1758N are shown in Fig. 2. Their quality is one of the best in our GMRT 325 MHz atlas (see Table 2). The left panel shows the total radio emission from the cluster central region imaged at full resolution overlaid on the optical image; the right panel shows the overlay between the Chandra X–ray image and the diffuse emission, after subtraction of the discrete point–like and extended sources S1 to S5 from the u–v data (see Section 2.2, Fig. 2 the left panel, and Table 3). The diffuse radio emission covers only a portion of the X–ray brightness distribution. It has a filamentary structure, and is aligned in the North–West/South–East direction. The radio and X–ray peaks of emission are in good spatial coincidence in the north–western part of the cluster, while a misplacement is clear in the south–eastern cluster region.

The total flux density of the diffuse emission, measured within the 3$\sigma$ contour, is $S_{\rm 325\ MHz} = 155 \pm 12$ mJy. The total size of this structure is ∼ 1.5 Mpc. The overall shape and size of the diffuse emission detected at 325 MHz is in reasonable agreement with the re–analysis carried out in G12. Giovannini et al. (2009) classify the radio emission as a radio halo and a double relic. Indeed the morphology of this source is very complex, however we find it difficult to disentangle possible different components. The overall spatial coincidence between the radio and X–ray emission, as clear from the right panel of Fig. 2, suggests that the source is centrally located. Hence, we consider it a giant radio halo.
The spectral index of the whole emission, using the total 1.4 GHz flux density reported in G12 ($S_{\rm 1.4\ GHz} = 23 \pm 5$ mJy, integrated over the same area) is $\alpha_{\rm 325\ MHz}^{\rm 1.4\ GHz} = 1.31 \pm 0.16$.

### 3.2. Clusters with halo and relics

Three clusters in the sample host multiple diffuse cluster sources. A 1300 and A 2744, both located at z∼0.3 and with similar X–ray luminosity, host a giant radio halo and a relic. They belong to the GMRT radio halo cluster sample, but being known radio halos they were not observed at 610 MHz in our earlier works (V07 & V08). RXCJ 1314.5–2515 hosts spectacular diffuse emission in the shape of a radio halo and two very long and symmetric relics.

#### 3.2.1. A 1300

A 1300 is located at z=0.308 and has $L_{\rm X,[0.1-2.4KeV]}$ = $1.4{\times}10^{45}$ erg s$^{-1}$. It hosts a radio halo, first reported in Reid et al. (1999, hereinafter R99) on the basis of radio observations carried out with the Molonglo Observatory Synthesis Telescope (MOST) at 843 MHz and with the Australia Telescope Compact Array (ATCA) from 1.34 GHz to 8.6 GHz. With a temperature of ∼ 11 keV (Pierre et al. 1997), A 1300 is one of the hottest clusters known. Optical and X–ray analysis (Pierre et al. 1997, Lemonon et al. 1997, Ziparo et al. 2012) suggest that it is a post–merger. The radio observations by R99 show that A 1300 is very active in the radio band. Beyond the radio halo, a relic is located in the south–western periphery of the cluster, and a number of radio galaxies with extended emission are found at the cluster centre. In a recent optical and X–ray analysis, Ziparo et al. (2012), reported on a possible shock front (consistent with a Mach number $M$=1.2±0.1) and on a sharp edge in the galaxy distribution at the location of the relic.

Due to strong interference, only the upper side band of the GMRT 325 MHz dataset could be used in our imaging process. Fig. 3 (left) shows the radio emission from the cluster centre (contours) at the intermediate resolution of 26.7″ × 18.1″, overlaid on the full resolution image (14.0″ × 8.8″), displayed in grey scale to highligt the position and morphology of the radio galaxies embedded in the diffuse cluster emission. The individual radio sources are labelled following the notation in R99 and their flux density is reported in Table 3. An elongated, thin structure, hereinafter referred as *bridge* (see inset in Fig. 3) connects the head–tail radio galaxy A2 to the point source A1. It is not clear whether such feature is an extension of the tail of A2 or a brightness peak of the diffuse radio halo. For this reason, Table 3 reports the flux density of A2 with and without the contribution of the *bridge*, which accounts for ∼18 mJy. Note that the radio sources labelled B2, B3 and 12 in R99 are undetected in our 325 MHz images, most likely due to their spectral slope. We subtracted the components of the individual radio galaxies (Table 3) from the u–v data (we considered the *bridge* as part of A2 and we subtracted it as well) and produced a low resolution image of the residual diffuse emission, which is shown in the right panel of Fig. 3, overlaid on the smoothed Chandra X–ray image. The 325 MHz brightness distribution of the radio halo is fairly uniform.

The shape of the radio halo at this frequency is similar to the higher frequency images, with the diffuse emission extending mainly East of the two radio sources A1 and A2. The overall size is also comparable to the one reported in R99, with a largest linear size (LAS) of ∼3.3′ (largest linear size LLS∼ 890 kpc). The S–W relic (B3 in R99), too, is similar in shape, extent and brightness distribution to

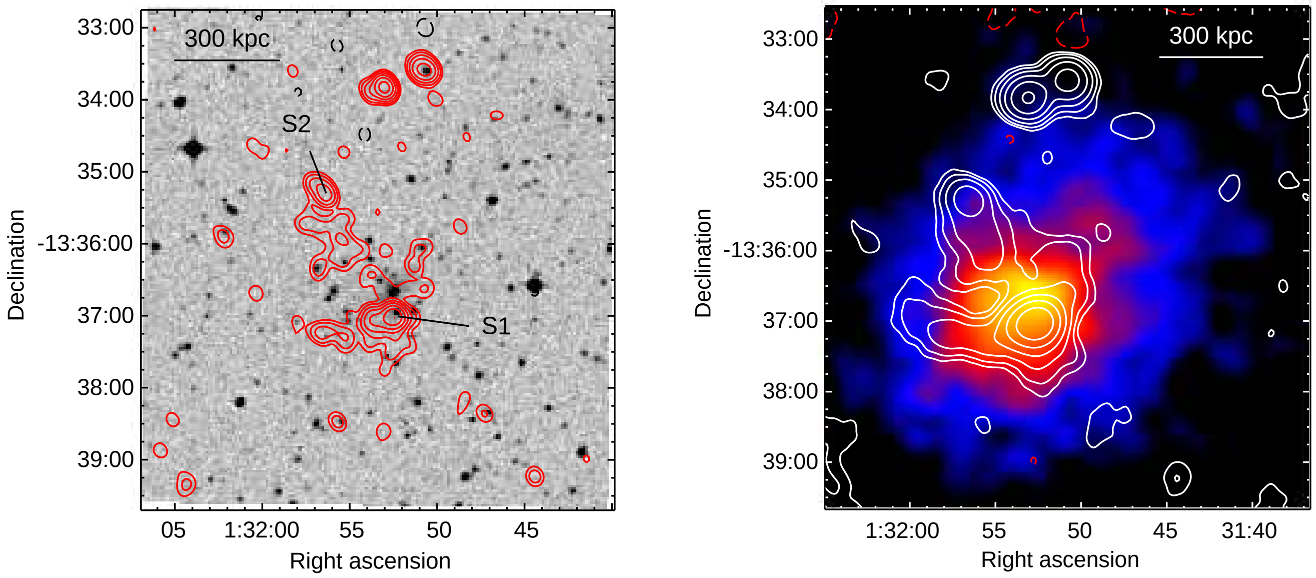

**Fig. 1.** *Left:* GMRT 325 MHz radio contours of A 209 at full resolution (11.0″ × 8.7″, p.a. 30°), overlaid on the optical POSS–2 image. The $1\sigma$ level in the radio image is 0.12 mJy beam$^{-1}$ and red contours are spaced by a factor 2 starting from $+3\sigma = 0.36$ mJy beam$^{-1}$. Black dashed contours correspond to the $-3\sigma$ level. Labels S1 and S2 show are the radio galaxies embedded in the radio halo emission. *Right:* GMRT 325 MHz radio contours at the resolution of 25.0″ × 25.0″, p.a. 0°, superposed to the smoothed Chandra X-ray image. No source subtraction has been performed. White contours start at $+3\sigma = 0.9$ mJy beam$^{-1}$ and then scale by a factor 2. The $-3\sigma$ level is shown as red dashed contours.

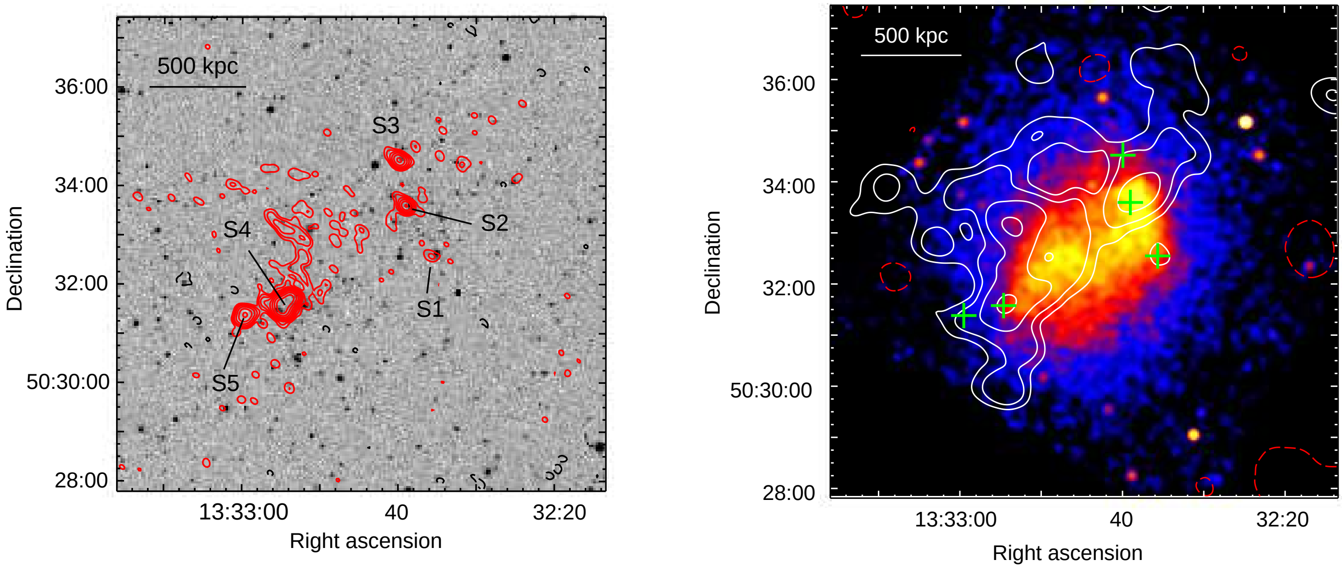

**Fig. 2.** *Left*: GMRT 325 MHz radio contours of the emission from A 1758N at the full resolution (10.5″ × 8.4″, p.a. 58°), overlaid on the POSS–2 red image. The $1\sigma$ noise level is 0.1 mJy beam$^{-1}$. Red contours start at 0.4 mJy beam$^{-1}$ and scale by a factor of 2. Black dashed contours correspond to the $-3\sigma$ level. Individual radio galaxies are labelled from S1 to S5. *Right*: 325 MHz contours of the giant radio halo overlaid on the smoothed Chandra X-ray image. The radio image has been obtained after subtraction of the discrete embedded sources (S1 to S5), whose position is marked as green crosses. The restoring beam is 35.0″ × 35.0″, p.a. 0°. The $1\sigma$ is 0.4 mJy beam$^{-1}$. White contours start at $+3\sigma = 0.12$ mJy beam$^{-1}$ and scale by a factor 2. The $-3\sigma$ level is shown as red dashed contours.

the earlier images, and its LLS at 325 MHz is ∼ 450 kpc. Our image shows the existence of an arc–shaped elongated feature, not visible in any of the images published in R99, located North–West of the cluster centre, which accounts for $S_{325\rm MHz} = 23 \pm 2$ mJy and is ∼ 700 kpc in extent. The overall morphology and location suggest that it might be another relic (see Fig. 3 right panel).

The total flux density measured in the radio halo, integrating within the $3\sigma$ contour level in Fig. 3 (right), is $S_{325\rm MHz} = 130 \pm 10$ mJy (the flux density of the *bridge* was not included). The flux density of the S–W relic is $S_{325\rm MHz} = 75 \pm 6$ mJy.

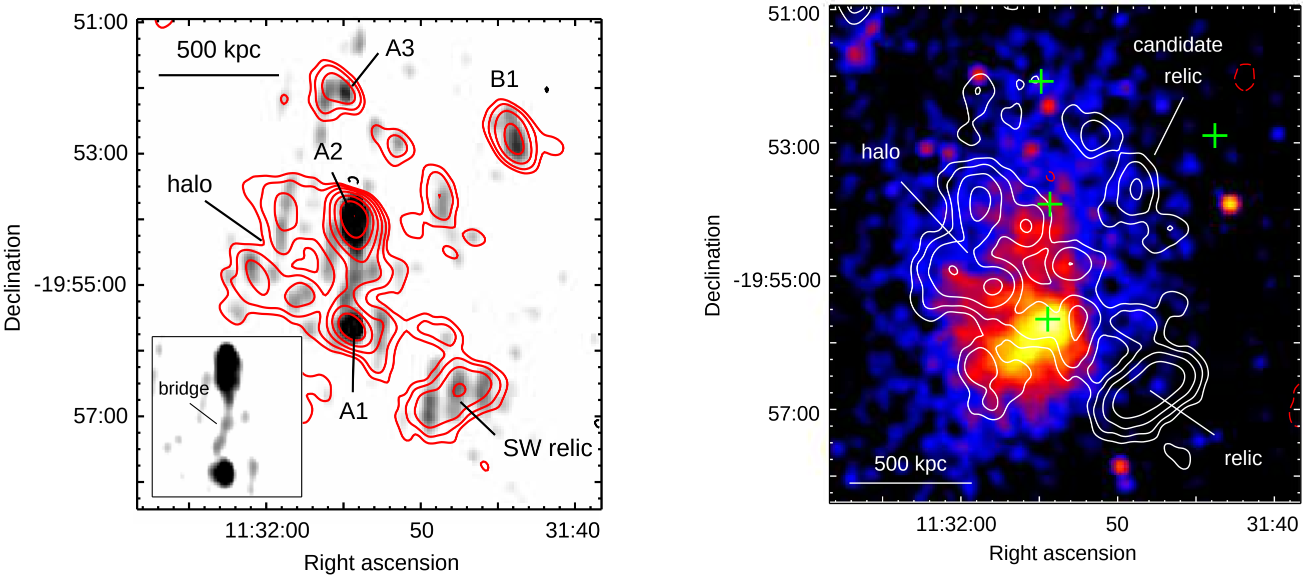

**Fig. 3.** *Left:* GMRT 325 MHz radio contours of the emission from A 1300 at the resolution of 27.6″ × 18.1″, p.a. 43°, overlaid on the grey scale full resolution image (14.0″ × 8.8″, p.a. 8°). The 1$\sigma$ noise level of the contour image is 0.6 mJy beam$^{-1}$. Red contours start at 1.8 mJy b$^{-1}$ and then scale by a factor of 2. The 1$\sigma$ noise level of the grey scale image is 0.45 mJy beam$^{-1}$. Individual radio galaxies are labelled following the notation in R99. *Right:* Radio contours of the central cluster region after subtraction of the discrete radio sources (the green crosses mark their location). The restoring beam is 28.0″ × 28.0″, p.a. 0°. The 1$\sigma$ is 0.5 mJy beam$^{-1}$. White contours start at 1.5 mJy beam$^{-1}$ and then scale by a factor of 2. The $-3\sigma$ level is shown as red dashed contours.

We combined our flux density values with those reported by R99 in the frequency range 843 MHz – 2.4 GHz to provide an estimate of the spectral index for the halo and the SW relic. The 1.36 GHz flux density of the radio halo reported in R99 is 10 mJy (consistent with the value we measured on the NVSS after subtraction of the contribution of the two embedded sources A1 and A2), which provides a spectral index $\alpha_{325\ \mathrm{MHz}}^{1.4\ \mathrm{GHz}}$=1.8. The inclusion of the bridge in the 325 MHz emission from the halo would further steepen the spectrum (up to $\alpha$=1.9). The S–W relic has $\alpha_{325\ \mathrm{MHz}}^{843\ \mathrm{MHz}}$=0.86, which steepens to $\alpha_{1.34\ GHz}^{2.4\ GHz} = 1.3$. We are aware that it is impossible to account for the different u–v coverages of the ATCA, MOST, GMRT and VLA. For this reason we regard these spectral considerations as indicative and we do not include this cluster in the discussion performed in Sect. 4.4.1.

The overlay in the right panel of Fig. 3 shows that the radio halo extends mainly North–East of the peak in the X–ray surface brightness. Both the S–W and the candidate relics are located at the border of the detected X–ray emission.

### 3.2.2. A 2744

A 2744 is located at the redshift z=0.3066 and has $L_{X,[0.1-2.4\mathrm{KeV}]} = 1.2 \times 10^{45}$ erg s$^{-1}$. The cluster hosts a well known spectacular diffuse radio emission, with a giant radio halo and a giant relic. VLA radio observations at 1.4 GHz and 327 MHz are reported in Govoni et al. (2001) and Orrú et al. (2007) respectively.
The cluster is a complex galaxy merger and has been studied in detail in a wide range of energy bands. Chandra observations (Kempner & David 2004) show that the cluster is formed by a main irregular component and a smaller subcluster to the North–West. The main cluster shows very complex substructure with a strong peak and a number of "ridges" in different directions. The subcluster is connected to the main one by a bridge of fainter X–ray emission, and its brigthtness distribution suggests that it is moving towards the main condensation (Kempner & David 2004). The very unrelaxed dynamical state of A 2744 is confirmed by optical spectroscopy, which reveals a redshift bimodal distribution and an unusually high merger velocity (Girardi & Mezzetti 2001). Merten et al. (2011) recently concluded that the main cluster and the subcluster are both post–mergers, and show properties similar to the Bullet cluster, with a misplacement between the gas and the dark matter.

Fig. 4 shows our 325 MHz GMRT images. Both the radio halo and the relic are already visible in the full resolution image (left panel). The two sources are connected by a faint bridge (right panel), visible also in the VLA 1.4 GHz image in Govoni et al. (2001). Thanks to the better sensitivity (∼ a factor of 3) of our image compared to the those in Orrú et al. (2007), the radio halo in A 2744 is larger than previously imaged at 325 MHz. In particular, we detect a north–western ridge, labelled in the right panel of Fig. 4, along the same direction of the subcluster X–ray emission. The largest linear size of the diffuse sources from the low resolution image (right panel) is LLS∼ 1.9 Mpc for the halo (including the NW ridge) and LLS∼1.3 Mpc for the relic. The bridge extends for ∼ 700 kpc between the halo and relic.

The radio/X–ray overlay in Fig. 4 (right) clearly shows that the emission from the radio halo extends over the whole X–ray emission, and beyond, with a positional shift between the X–ray and radio peaks both for the main cluster and for the N–W subcluster. The radio brightness distribution is asymmetrically peaked, and the southern part

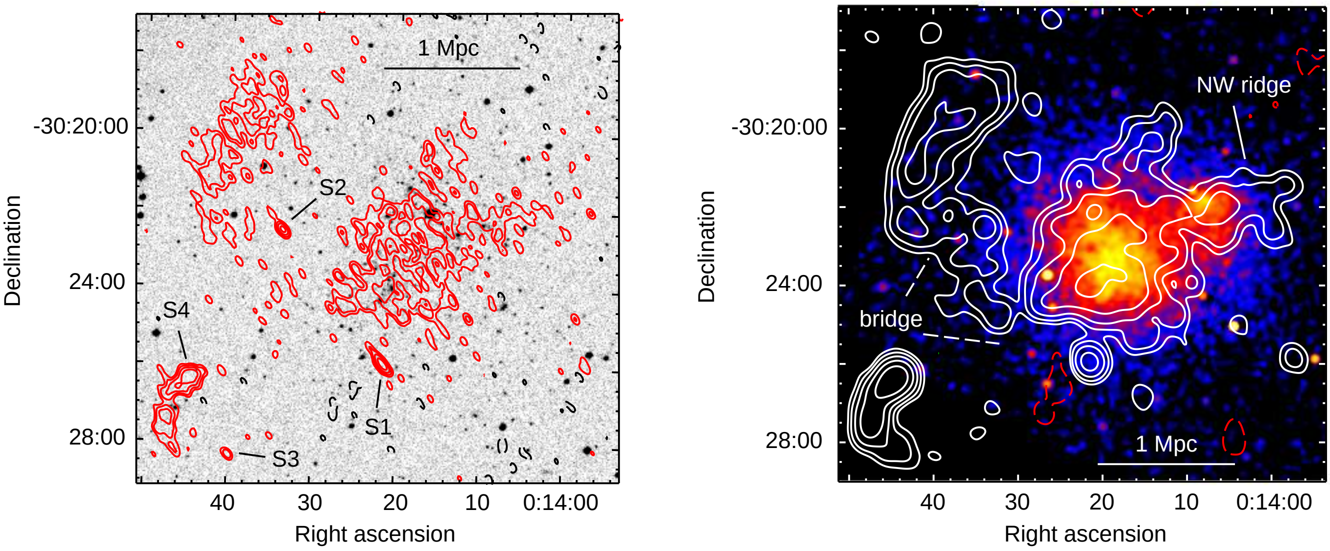

**Fig. 4.** *Left*: GMRT 325 MHz radio contours of A 2744 at the full resolution of 15.9″ × 8.5″, p.a. 38°, overlaid on the POSS–2 red image. The $1\sigma$ noise level is 0.15 mJy beam$^{-1}$. Red contours start at 0.5 mJy beam$^{-1}$ and then scale by a factor of 2. Dashed, black contours correspond to the $-3\sigma$ level. Individual radio galaxies are labelled from S1 to S4. *Right*: Low resolution (35.0″ × 35.0″, p.a. 0°) radio contours overlaid on the smoothed Chandra X–ray image. The $1\sigma$ noise level in the radio image is 0.35 mJy beam$^{-1}$. White contours start at 1 mJy beam$^{-1}$ and then scale by a factor of 2. The $-3\sigma$ level is shown as dashed, red contours.

of the radio halo is edge sharpened. It is noteworthy that Markevitch (2010) recently reported on the detection of a X–ray surface brightness edge, suggesting the presence of a shock front, at the location of this radio edge sharpening. The front has been confirmed by the Chandra analysis presented by Owers et al. (2012), who derived a Mach number of $M$=1.4 for the shock (see Fig. 12 in Markevitch 2010 for a radio/X–ray overlay of the shock region). Similar radio/X–ray spatial correlations have been observed in few other clusters with a giant radio halo, e.g., A 520 (Markevitch et al. 2005) and A 754 (Macario et al. 2011a).

As it is commonly found, the relic has a higher surface brightness compared to the halo, and its size is in agreement with the literature images. The radio/X–ray overlay confirms that the relic is located just outside the region where significant X–ray emission is detected (see also Govoni et al. 2001).

From the low resolution image we measured a total flux density $S_{325\ \mathrm{MHz}} = 323 \pm 26$ mJy for the halo (excluding the bridge and source S1), and $S_{325\ \mathrm{MHz}} = 122 \pm 10$ mJy for the relic (excluding the bridge and source S2). The flux density in the bridge is ∼ 30 mJy. The measurements were taken within the $3\sigma$ contour level. Both values are considerably higher than those reported in Orrú et al. (2007).

A 2744 is included in the re–analysis carried out in G12. Using their 1.4 GHz flux density values over the same area, i.e. $S_{1.4\ \mathrm{GHz}} = 57 \pm 3$ and 20±1 mJy respectively for the halo and for the relic, we obtain $\alpha = 1.19^{+0.08}_{-0.11}$ for the halo, and $\alpha = 1.24 \pm 0.10$ for the relic.

### 3.2.3. RXCJ 1314.4–2515

The cluster RXCJ 1314.4-2515 (z=0.244, $L_{X,[0.1-2.4\mathrm{KeV}]} = 1.1 \times 10^{45}$ erg s$^{-1}$) is a spectacular example of a major merger with a massive subcluster (Valtchanov et al. 2002). In was the first cluster where a radio halo and two relics were discovered (Feretti et al. 2005, V07). So far only two clusters with such features have been found (CIZA J 2242.8+5301, van Weeren et al. 2011b; MACS J 1752.0+4440, van Weeren et al. 2012). The two relics are elongated, Mpc-size structures located in opposite directions with respect to the cluster centre. Deep XMM–Newton observations led to the discovery of a prominent shock front, with Mach number M∼ 2.5, remarkably coincident with the outer border of the western relic and likely produced by the merger of the cluster with a massive subcluster (Mazzotta et al. 2011).

Our GMRT 325 MHz observations were affected by a number of antenna failures and strong interference, nevertheless we managed to image the brightest features of the diffuse emission. The 325 MHz cluster radio emission is reported in Fig. 5, where the full resolution image is overlaid on the optical frame (left) and a tapered image (26″ × 10″) is overlaid on the smoothed XMM-Newton image (right).

Due to the poor quality of our dataset, both relics are considerably smaller in size compared to the 610 MHz images published in V07 and to the VLA 1.4 GHz images in Feretti et al. (2005). In the light of all this, the flux density values reported in Tab. 4 should be considered as lower limits, and any spectral consideration is deferred to a detailed ongoing multifrequency study (Giacintucci et al. in progress).

## 3.3. *Clusters with complex diffuse emission*

### 3.3.1. A 1682: a very complex cluster

A 1682 (z=0.226, $L_{X,[0.1-2.4\mathrm{KeV}]} = 7.0 \times 10^{44}$ erg s$^{-1}$) is a merging massive cluster (Morrison et al. 2003) with very complex radio emission. High sensitivity and high resolution observations in the radio band (GMRT at 610 MHz) were first published in V08, and show that the central com-

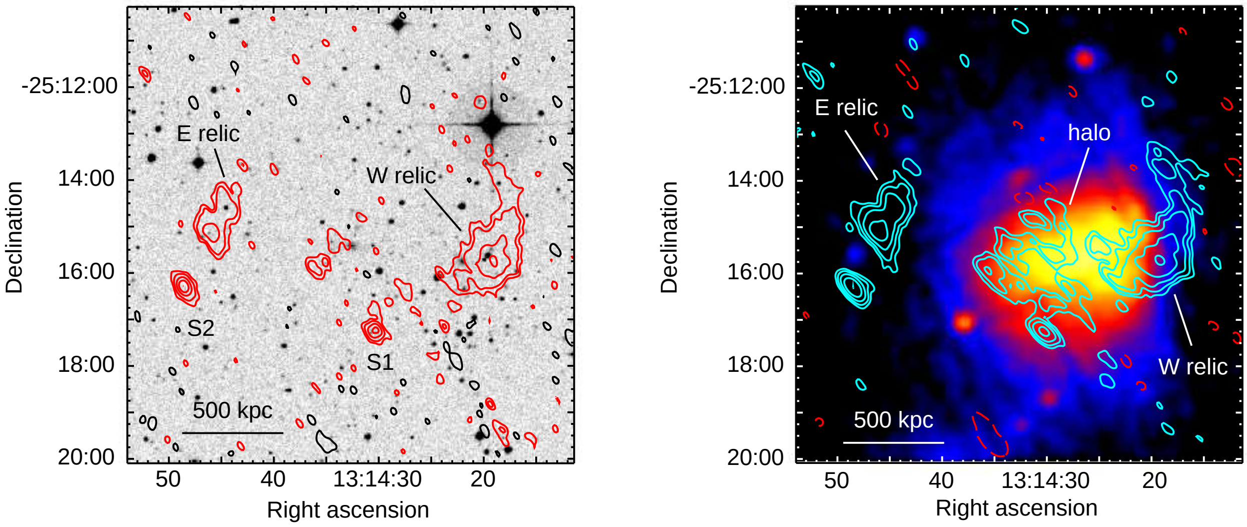

**Fig. 5.** *Left*: GMRT 325 MHz image of RXCJ 1314.4–2515 at the resolution of 15.1″ × 8.0″, p.a. 32°, overlaid on the POSS–2 red image. The 1$\sigma$ noise level is 0.16 mJy beam$^{-1}$. Red contours start at 0.5 mJy beam$^{-1}$ and then scale by a factor of 2. Black contours correspond to the $-3\sigma$ level. Individual radio galaxies are labelled S1 and S2. *Right:* GMRT 325 MHz radio contours overlaid on the smoothed XMM–Newton X–ray image. The resolution of the radio image is 26.1″ × 10.2″, p.a. 43°. The 1$\sigma$ noise level in the radio image is ∼0.2 mJy beam$^{-1}$. Cyan contours start at 0.6 mJy beam$^{-1}$ and then scale by a factor of 2. The $-3\sigma$ level is shown as red dashed contours.

pact emission visible on the NVSS is actually a blend of a number of features: *(a)* a strong radio galaxy, associated with the dominant $m_g$=18.0 galaxy at the cluster centre (z=0.21839, Koester et al. 2007), which diffuses into a tail; *(b)* two filamentary structures of unclear origin, which were named *S–E* and *N–W ridges* in V08; *(c)* diffuse excess emission over a ∼ Mpc–size region, suggestive of the presence of an underlying giant radio halo.

Our 240 MHz images are reported in Fig. 6. The left panel shows the full resolution contours overlaid on the optical emission (red plate of the Digitized Sky Survey DSS–2), while in the right panel a tapered image is overlaid on the 74 MHz emission visible on the VLA Low–Frequency Sky Survey (VLSS). The N–W ridge extends ∼ 2′, i.e. ∼ 430 kpc, while E–tail is ∼ 380 kpc. The S–E ridge is ∼ 1′, i.e. ∼ 220 kpc. The brightness distribution of both the N–W and S–E ridge is centrally peaked all over their extent. Fig. 6 clearly shows the presence of a new component beyond the features already visible at 610 MHz, labelled as "diffuse component" (right panel), and coincident with a similar feature on the VLSS. This component is a prominent feature also in GMRT 150 MHz images (Macario et al. 2012) and in LOFAR (LOw Frequency ARray) observations (Macario et al. in prep.).

From the low resolution image in the right panel of Fig. 6 we measured the 240 MHz flux density of the various components, and obtained: $S_{(\rm N-W\ ridge)} = 468 \pm 23$ mJy; $S_{(\rm E-tail)} = 1126 \pm 56$ mJy (this value includes both the brightest part of the emission and the long tail, while the contribution of S2, associated with a 18.0 magnitude cluster galaxy at z=0.233, Hao et al. 2010, has been removed); $S_{(\rm S-E\ ridge)} = 63 \pm 4$ mJy; $S_{(\rm Diff\ Comp)} = 46 \pm 4$ mJy.

The left panel of Fig. 7 shows an overlay of the radio emission of A 1682 at 610 MHz (V08) and 240 MHz. The shape, size and brightness distribution of the E–tail, the N–W and the S–E ridges are in very good agreement at the two frequencies.

In order to throw some light on the nature of the various components of the diffuse radio emission in this cluster, we performed a spectral study between 610 MHz and 240 MHz. The total spectral index of the N–W ridge, E–tail and S–E ridge between 610 MHz and 240 MHz, derived using images with resolution ∼ 14″ and computed integrating over the same area, are respectively: $\alpha_{\rm 240\ MHz}^{\rm 610\ MHz}\ ({\rm N-W\ rigde}) = 1.62 \pm 0.09$, $\alpha_{\rm 240\ MHz}^{\rm 610\ MHz}\ ({\rm E-tail}) = 0.99^{+0.09}_{-0.10}$, $\alpha_{\rm 240\ MHz}^{\rm 610\ MHz}\ ({\rm S-E\ rigde}) = 1.53^{+0.11}_{-0.13}$. The spectrum of E–tail actually consists of two distinct components: the brightest part of the emission (before the radio emission bends) has a "normal" spectrum, i.e. $\alpha = 0.78$, typical of radio galaxies, while the spectrum in the long tail is very steep, with $\alpha = 2.1$.
We point out that the 610 MHz observations we are using for this analysis do not belong to the same set of observations of the GMRT Radio Halo survey, but they are part of a longer exposure carried out two years after the survey observations. While it is still possible that the 610 MHz flux density measurements are underestimated (see Macario et al. 2010), a check on the S–E ridge does not suggest any missing flux at 610 MHz. The spectral index for this feature between 240 MHz and 610 MHz is consistent with that reported in V08 between 610 MHz and 1.4 GHz (NVSS).

To check for steepness gradients in the N–W ridge and in the E–tail we matched the u–v coverage of the 610 MHz and 240 MHz datasets and produced a spectral index image of the central cluster region at the resolution of 12″ × 10″. Our results are given in the right panel of Fig. 7. The distribution of $\alpha_{\rm 240\ MHz}^{\rm 610\ MHz}$ in the N–W ridge shows a gradient parallel to the source major axis, from ∼ 1 (dark blue) to ∼ 2.3 (light green) going from East to West. In the E–tail two distinct regions are clearly visible: (1) the spectral index shows a gradient at the South–Western end of the structure, with $\alpha_{\rm 240\ MHz}^{\rm 610\ MHz}$ steepening from ∼ 0.5 at the location of the dominant double radio galaxy, to ∼ 1.2 where the feature bends; (2) after the bending the spectral index is in the range 1.8–2.2 with a patchy distribution.

To investigate the possible connection between the double radio source associated with the dominant cluster galaxy and the E–tail, we re–analysed two short archival VLA observations at 1.4 GHz with the array in the A and D configuration (projects AM699 and AM469 respectively). The VLA–A array image at the resolution of $1''$ is reported in the inset in the left panel of Fig. 7. It is clear that the BCG is a compact double, whose lobes bend on the S–W direction on an angular scale of $\sim 5''$. Such bending seems unrelated with the E–tail. The spectral index distribution along the E–tail seems to support this idea: no steepening is found moving away from the nuclear emission, as it would be expected for a tailed radio galaxy.

The diffuse component south–east of the cluster centre is a new intriguing feature. It has the steepest spectrum. Comparison of the 240 MHz and 74 MHz flux density values is difficult, since the VLSS image provides very different values depending on the algorithm used to integrate over that portion of the image. Considering the flux density measured at 610 MHz over the same region, we obtain a spectral index $\alpha_{610\ \mathrm{MHz}}^{240\ \mathrm{MHz}} = 2.09 \pm 0.15$. Finally, in V08 we reported on the presence of residual flux density in a cluster region of $\sim$ 1 Mpc within the centre at 610 MHz. We find a similar situation also at 240 MHz. In Venturi et al. (2011b) we carried out an analysis of this residual emission after subtraction of the individual sources from the u–v data, following a procedure similar to that adopted for A 781 (Venturi et al. 2011a). Excess flux density is confirmed at both frequencies and at 1.4 GHz.

To summarize, the radio emission at the centre of A 1682 is very complex, and the nature of the various features remains enigmatic. In particular:

*(a)* The size, morphology and spectrum of the N–W ridge are consistent with our knowledge of relic sources, however the spectral gradient between 610 MHz and 240 MHz would suggest some merger activity from West to East, which is not confirmed by the current X–ray data (see Fig. 7 in V08).

*(b)* On the basis of the high resolution VLA–A image of the BCG and on the spectral index distribution (Fig. 7), it seems unlikely that the E–tail is associated with the BCG, but at present there are no alternative suggestions for its origin. We note that the small scale radio emission of the BCG hints at a motion in the Southwest–Northeast direction.

*(c)* The size of the S–E ridge is only $\sim$ 220 kpc, and it is considerably smaller than the relics known so far.

*(d)* The nature of the diffuse component is unclear. One possibility is that it is the brightest part of an underlying steep spectrum radio halo. Alternatively, it could be a dying radio galaxy.

A detailed multifrequency study of this cluster, based on deep observations at 74 MHz (VLA–A, Venturi et al. 2011b), at 150 MHz (GMRT, Macario et al. 2012) and 325 MHz (GMRT), will allow to us classify the diffuse extended sources and throw a light on their nature (Dallacasa et al. in preparation).

### 3.4. Z 2661

Z 2661 is the second most luminous cluster in the GMRT Radio Halo Cluster sample, with $L_{X,[0.1-2.4\mathrm{KeV}]} = 1.78 \times 10^{45}$ erg s$^{-1}$. V08 reported the presence of very faint candidate diffuse emission at the cluster centre ($S_{610\ \mathrm{MHz}} \sim 5.9$ mJy). Our 325 MHz observations failed to detect diffuse emission. Fig. 8 shows the central cluster region at two different resolutions. Only the radio emission from the individual sources is clearly detected, and no significant excess flux density is measured over the same region covered by the diffuse emission at 610 MHz.

### 3.5. The remaining clusters in the sample

In this section, for completeness and to help the discussion, we briefly summarize the most important radio properties of the four clusters followed up with the GMRT at 325 MHz and 240 MHz (Table 1), already published in separate papers.

#### 3.5.1. A 521: the prototype ultra-steep spectrum radio halo

The low frequency observations of A 521, carried out at 240 MHz and 325 MHz to study the cluster relic (Giacintucci et al. 2008), led to the discovery of a very steep spectrum giant radio halo at the cluster centre (Brunetti et al. 2008). The source was detected in very deep 1.4 GHz VLA observations (Dallacasa et al. 2009), which provided $\alpha_{240\ \mathrm{MHz}}^{1.4\ \mathrm{GHz}} = 1.86 \pm 0.08$, and further imaged with the GMRT at 150 MHz (Macario et al. 2012). The spectrum of the relic is a power law with $\alpha_{240\ \mathrm{MHz}}^{4.8\ \mathrm{GHz}} = 1.48$ (Giacintucci et al. 2008).

#### 3.5.2. The ultra–steep spectrum radio halo in A 697

The GMRT 325 MHz observations of the faint radio halo in A 697 detected at 610 MHz (V08) revelaed that it is another example of very steep spectrum source. The 325 MHz images and a detailed study of the radio halo and the properties of the hosting cluster were presented in Macario et al. (2010), who reported a flux density value $S_{325\ \mathrm{MHz}} = 47.3 \pm 2.7$ mJy and a spectral index $\alpha_{325\ \mathrm{MHz}}^{1.4\ \mathrm{GHz}} = 1.8 \pm 0.1$. This value is in line within the errors with the analysis carried out in van Weeren et al. (2011), who reported $\alpha = 1.64 \pm 0.06$ on the basis of deep 1.4 GHz images. The steep spectrum has been confirmed by the analysis of GMRT 150 MHz data (Macario et al. 2011b; Macario et al. 2012). The linear size of the source at this frequency is $\sim$ 1.3 Mpc, considerably larger than at higher frequencies. This giant radio halo has a smooth surface brightness over its all extent. Literature X–ray and optical data suggest that the cluster is unrelaxed, and even though the available information does not allow a detailed study, either a multiple merger or a major merger along the line of sight are the possible scenarios.

#### 3.5.3. Complex radio emission in A 781

A 781 is an intriguing case. Beyond a number of individual galaxies, the central part of the cluster is dominated by a diffuse source located at the border of the X–ray emission,

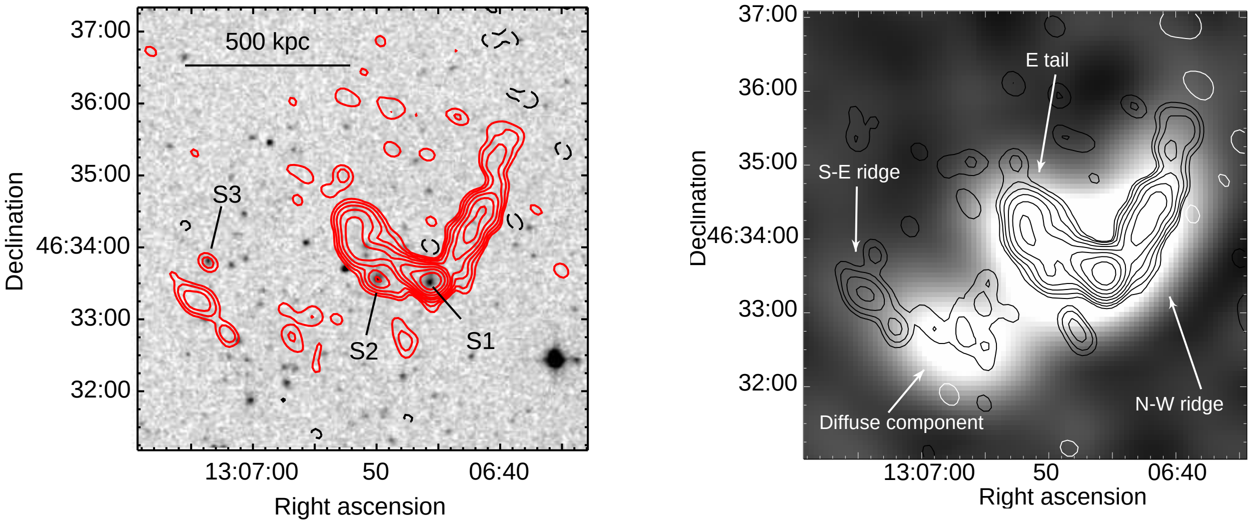

**Fig. 6.** *Left*: GMRT 240 MHz image of A 1682 at the resolution of 12.5″ × 9.2″, p.a. 55.7°. The 1$\sigma$ rms in the image is 0.6 mJy beam$^{-1}$. Red contours start at 2 mJy beam$^{-1}$ and scale by a factor of 2. Black dashed contours correspond to the $-2$ mJy beam$^{-1}$ level. Individual radio galaxies are labelled S1, S2 and S3. The optical image is the red plate of the Digitized Sky Survey (DSS–2). *Right*: GMRT 240 MHz contours overlaid on the VLSS 74 MHz emission (grey scale). The resolution of the 240 MHz image is 18.3″ × 14.0″, p.a. 21.7°. Black contours start at 2 mJy beam$^{-1}$ ($1\sigma = 0.6$ mJy beam$^{-1}$) and are spaced by a factor of 2. White contours correspond to the $-2$ mJy beam$^{-1}$ level.

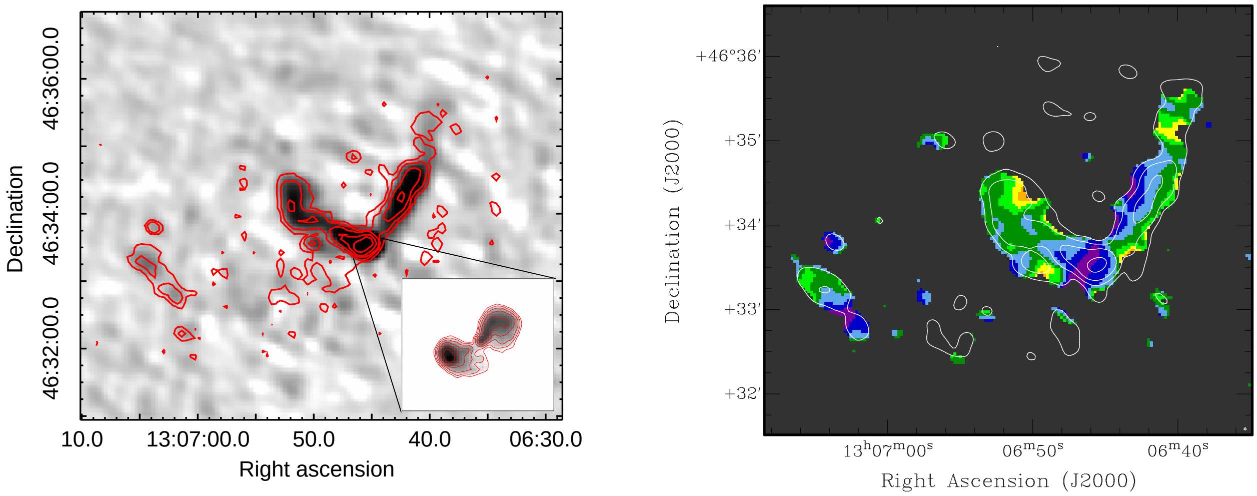

**Fig. 7.** *Left*: GMRT 240 MHz grey scale image of A 1682 with 610 MHz contours overlaid. The 240 MHz image is the same as Fig. 6, right panel. The resolution of the 610 MHz image is 6.2″ × 4.1″, p.a. 61.2°, the 1$\sigma$ rms in the image is 25 $\mu$Jy beam$^{-1}$, the first contour is 0.1 mJy beam$^{-1}$, and contours are spaced by a factor of 4. The inset in the bottom right corner is the 1.4 GHz VLA–A image of the central BGC at the resolution of 1.1″ × 1.1″. Contours are spaced by a factor of 2 starting from 0.15 mJy beam$^{-1}$. *Right*: Spectral index image of A 1682, with GMRT 240 MHz contours overlaid (resolution 12″ × 10″, p.a. 60°) The first contour is 3 mJy beam$^{-1}$, contours are spaced by a factor of 4. The spectral index scale ranges from light green ($\alpha_{240\ \mathrm{MHz}}^{610\ \mathrm{MHZ}} \sim 2.3$) to violet ($\alpha_{240\ \mathrm{MHz}}^{610\ \mathrm{MHZ}} \sim 0.5$).

classified as a radio relic with spectrum $\alpha_{325\ \mathrm{MHz}}^{1.4\ \mathrm{GHz}} = 1.25 \pm 0.06$ (V08; Venturi et al. 2011a).

On the basis of a detailed radio/X–ray analysis carried out by Cassano et al. (2010), the cluster was classified as "outlier" in the quantitative correlations relating cluster mergers and the presence of a radio halo: the cluster shows a high degree of disturbance but lacks a radio halo. Our GMRT 325 MHz follow–up observations revealed the presence of residual emission at the cluster centre, after subtraction of the individual sources (Venturi et al. 2011a). Such excess flux density sums up to $\sim 20$ mJy and is visible at the 2$\sigma$ level. Our findings did not confirm the 1.4 GHz detection of the radio halo claimed in Govoni et al. (2011), unless the source has an unplausibly flat spectrum ($\alpha_{325\ \mathrm{MHz}}^{1.4\ \mathrm{GHz}} \leq 0.5$, see Venturi et al. 2011a for a complete discussion).

An attractive possibility is that the residual emission reveals the presence of an underlying very low surface brightness radio halo. Allowing for all the uncertainties in our analysis, an accurate comparison between the 325 MHz and

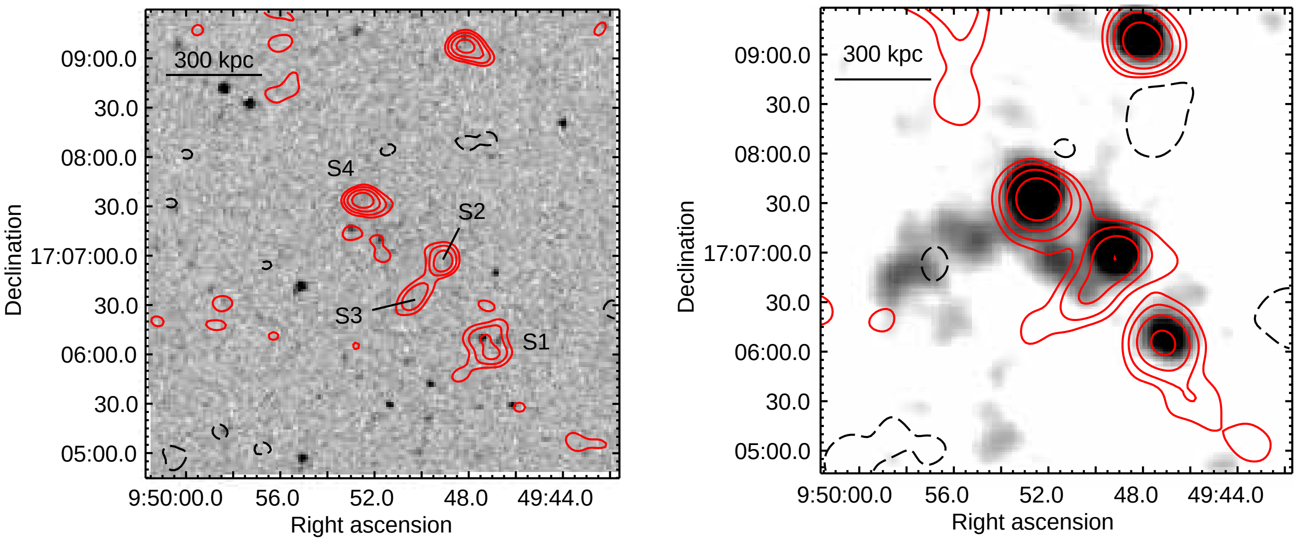

**Fig. 8.** *Left*: GMRT 325 MHz radio contours of the emission from Z 2661 at the full resolution ($10.8'' \times 8.4''$, p.a. $-83°$), overlaid on the POSS–2 red image. The $1\sigma$ noise level is 0.12 mJy beam$^{-1}$. Red contours start at 0.36 mJy beam$^{-1}$ and then scale by a factor of 2. Black dashed contours correspond to the $-3\sigma$ level. Individual radio galaxies are labelled from S1 to S4. *Right*: 325 MHz contours at the resolution of $25.0'' \times 25.0''$, p.a. 0°, overlaid on the GMRT 610 MHz image ($17.7'' \times 17.4''$) from V08. Red contours start at $+3\sigma$ =0.6 mJy beam$^{-1}$ and then scale by a factor 2. The $-3\sigma$ level is shown as black dashed contours. The rms noise level in the 610 MHz image is 65 $\mu$Jy beam$^{-1}$.

610 MHz images suggests that the 325 MHz residuals could be consistent with a diffuse source with spectrum steeper than $\alpha > 1.5$.

#### 3.5.4. RXCJ 2003.5−2323

The cluster is one of the most distant in our sample (z=0.317) and hosts a giant radio halo (LLS$\sim$1.4 Mpc), discovered with the GMRT at 610 MHz (V07). The cluster been extensively followed–up by us in the radio, X–ray and optical band (Giacintucci et al. 2009).

The radio halo is very powerful, and its spectrum can be well fitted by a single power law with spectral index $\alpha^{\rm 1.4GHz}_{\rm 240\ MHz} = 1.27^{+0.18}_{-0.08}$. It has a regular shape and its size is very similar from 240 MHz to 1.4 GHz. Its brightness distribution is characterised by clumps and filaments. Our multiwavelength study supports the scenario of a merger–driven formation for this giant radio halo.

## 4. Discussion

The main goal of our GMRT 325 MHz follow–up program of the halos, relics and candidates in the GMRT cluster sample (i.e. redshift range z=0.2–0.4, X–ray luminosity $L_{\rm X}0.1-2.4$ keV $> 5\times10^{44}$ergs$^{-1}$, $\delta > -30°$, V07 and V08) was to perform high sensitivity imaging of diffuse cluster sources at a key frequency for our understanding of their origin. Both halos and relics are easily detected at 325 MHz, due to their steep spectrum and increased brightness with respect to the GHz observing frequencies. Compared to the few other interferometers operating at frequencies of the order of few hundred MHz, the GMRT has the advantage to allow accurate subtraction of the individual sources usually embedded in the diffuse emission, thus allowing a much more precise flux density measurement of the diffuse cluster sources, as well as much more reliable imaging of their fine scale features. This is critical to perform a detailed comparison with the distribution of the X–ray emission, and to derive reliable integrated spectra. As a matter of fact, integrated spectra of radio halos still suffer from many uncertainties, mainly due to the miscellanoeus collection of data, i.e. different arrays, resolutions, and procedures in the subtraction of individual embedded sources (see Venturi 2011).

Observations at frequencies $\nu \leq$ 325 MHz clearly show that the diffuse radio emission in galaxy clusters is very complex: new features show up, beyond the canonical classification of radio halos and relics, and the appearance of radio halos may change with frequency, both in some morphological details, and in the overall size. Some of the most relevant findings in our work are summarized and discussed in the following sections.

### *4.1. Morphology of radio halos*

#### 4.1.1. Size versus frequency

Our results clearly show that our view of radio halos changes at low frequencies. In some cases, the size of radio halos is very similar going from 1.4 GHz down to 325 MHz and 240 MHz. A clear example is RXCJ 2003.5–2323 (Giacintucci et al. 2009), and to a less extent A 2744. The total size of A 1300 is similar in our image and those in R99, even though the different angular resolution and sensitivity do not allow an accurate comparison.

On the other hand, some radio halos with spectral index steeper than $\alpha^{\rm 1.4\ GHz}_{\rm 325\ MHz} > 1.6$ (see also next section) are more extended at frequencies of few hundred MHz, being barely detected at 1.4 GHz, as is the case for A 521 (Dallacasa et al. 2009).

While it is tempting to suggest that the "GHz halos", i.e. those with "normal" ($\alpha \sim 1.2 \div 1.3$) spectrum, tend to have size and shape similar at all frequencies, and the "low frequency halos", i.e. those with very steep spectrum ($\alpha \geq 1.6$)

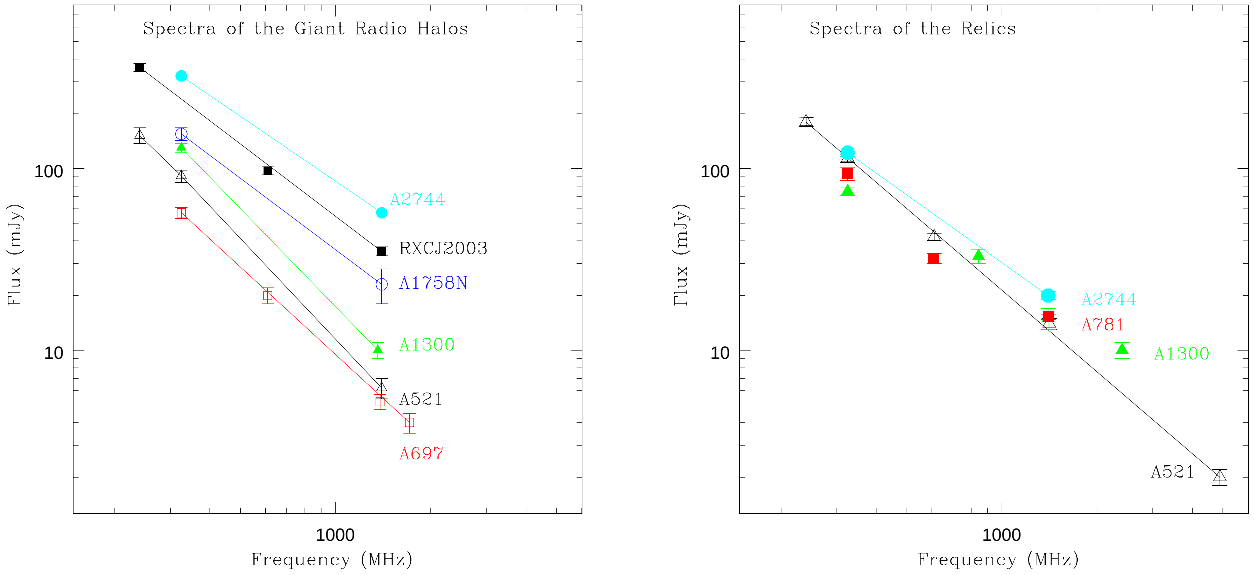

**Fig. 9.** *Left*: Spectra of the giant radio halos in the GMRT Radio Halo Survey. The 325 MHz data points are reported in Table 4. The remaining data are taken from: A 697 Macario et al. (2010) and van Weeren et al. (2011); A 521 Brunetti et al. (2008); RXCJ2003.5–2323 Giacintucci et al. (2009). For A 1300 see Sect. 3.2.1; for A 1758N see Sect. 3.1.2; for A 2744 see Sect. 3.2.2. *Right*: Spectra of relics from the GMRT Radio Halo Survey. The 325 MHz data points are reported in Table 4. The remaining data are taken from: A 521 G08; A 781 Venturi et al. (2011a); A 1300 R99; A 2744 see Sect. 3.2.2. In both panels the lines are drawn to help the visual inspection and are not the best fit power law.

show increasing size at decreasing frequency, as is the case for A 697 (see Macario et al. 2010 and 2011b, and van Weeren et al. 2011), it is possible that this difference is the result of the limited sensitivity of the current interferometers. The improved sensitivity of the EVLA at GHz frequencies and of the LOFAR below 240 MHz will allow to carefully address this point, and explore the possibility that the dependence of the size with frequency is the result of the radial spectral steepening.

#### 4.1.2. The brightness distribution and radio/X comparison

An important outcome of our 325 MHz survey concerns the brightness distribution of radio halos, which differs from case to case: A 697 is centrally peaked; A 2744 is asymmetrically peaked; most halos have a rather “clumpy” brightness distribution (A 521, Brunetti et al. 2008; A 1300; A 1758N; RXCJ 2003.5–2323, Giacintucci et al. 2009). Other known clusters in the literature show similar properties: the Coma cluster is centrally peaked (see for instance the 325 MHz image reported in Brown & Rudnick 2011), while A 754 is clumpy (Macario et al. 2011a).

The comparison of the radio and X–ray brightness distribution provides further insightful information. “Clumpy” radio halos are usually found in clusters with inhomogeneous X–ray distribution, as is the case for A 521, A 1300 (see right panel of Fig. 3) and RXCJ 2003.5–2323. On the other hand, the peak in the radio halo brightness distribution may coincide with the thermal peak, as is the case for A 697 (Macario et al. 2010), or be misplaced from it, as it is clear in A 1758N and A 2744 (right panel of Figs. 2 and 4 respectively).

These observational differences may contain important information of the type of merger and on the interplay between the cluster dynamical activity and the non–thermal emission. This result should be taken into account when addressing the origin of radio halos.

### 4.2. Integrated spectra of halos and relics

One of the most outstanding results of our low frequency follow–up of the GMRT Radio Halo survey has been the discovery of ultra–steep spectrum radio halos, i.e. A 521 and A 697 (see Sections 3.5.1 and 3.5.2 respectively). To highlight the different spectral slope of the spectrum of these two clusters compared to the others surveyed with the GMRT at 325 MHz, in the left panel of Fig. 9 we report the spectra of the giant radio halos in A 2744, A 521, A 697, A 1300, A 1758N, RXCJ 2003.5–2323. It is worth pointing out that A 521, A 697 and RXCJ 2003.5–2323 have been analysed using the same approach on the datasets at all frequencies. This is critical if we consider all the uncertainties in the subtraction of the contribution of individual sources embedded in the diffuse radio emission. The lines are not the best fit, and are drawn only to help the visual inspection.

Even considering only the clusters in the GMRT sample, it is clear that the observed spectral index of radio halos is quite different from case to case, and it goes from $\alpha_{325\ \mathrm{MHz}}^{1.4\ \mathrm{GHz}} \sim 1.2$ (A 2744) to $\sim 1.9$ (A 521), with a spread of at least $\Delta\alpha \sim 0.7$. This reflects into a spread in the energy distribution of the relativistic particle population of the order $\Delta\delta^{e^{\pm}} \sim 1.4$, which needs to be explained. One possibility is that a variety of mechanisms produces relativistic particles with different energy distributions. More likely, the broad range of observed synchrotron spectra suggests that the spectrum of the relativistic particles is not a power law, and that it is the result of the combined effect of a high energy break in the electron energy distribution and an inhomogeneous magnetic field over the cluster volume. A break in the spectrum of the emitting particles is predicted by turbulent re–acceleration models, or more generally, when the time scale of particle re-acceleration is comparable to that of radiative losses ($10^7$–$10^8$ years).

The observational properties of the relics in the GMRT radio halo survey (A 521, A 781, A 1300, A 2744) are more homogeneous. In all cases their morphology, brightness distribution and extent are fairly consistent at all frequencies. The only exception is A 781, which is more extended at 325 MHz, compared to 610 MHz and 1.4 GHz (Venturi et al. 2011a). The spectral index $\alpha_{325\ \mathrm{MHz}}^{1.4\ \mathrm{GHz}}$ is in the range 1.25 (A 781) – 1.48 (A 521).
We do not include the double relic cluster RXCJ 1314.4–2515 in these spectral considerations, due to the poor quality of the 325 MHz images. This cluster has been reobserved with the GMRT at 325 MHz and a separate paper is in progress (Giacintucci et al. in prep). The spectral index between 610 MHz and 1.4 GHz is $\alpha_{610\ \mathrm{MHz}}^{1.4\ \mathrm{GHz}} = 1.40 \pm 0.09$ and $1.41 \pm 0.09$ for the western and eastern relic respectively (V07).
In the right panel of Fig. 9 we report the spectra of the relics in A 2744, A 521, A 781, A 1300. The spread in flux density for these sources is much narrower compared to halos. The lines are drawn to help the visual inspection. Due to the small number of available relic radio spectra we cannot conclude that this is a general behaviour.

### 4.3. Diffuse cluster emission beyond halos and relics

A number of diffuse sources, which do not fit either into the radio halo or relic class, have been detected in some clusters. Our findings are summarized here below.

- A clear “bridge” of emission connects the radio halo and the relic in A 2744 (right panel of Fig. 4) and in RXCJ 1314.4–2515 (V07); a similar feature is visible in A 521 (Brunetti et al. 2008) and A 1300 (right panel of Fig. 3) in the region between the halo and the relic. Radio bridges have been so far observed only in very few famous cases, such as the Coma cluster (Kim et al. 1989; Brown & Rudnick 2011) and A 3667 (Carretti et al. 2012). Projection effects cannot be ruled out, however an attractive explanation for these features assumes that they may origin from merger shock re–accelerated electrons, which move downstream as the shock advances through the ICM and are further accelerated by the turbulence injected by the merger in the ICM closer to the cluster centre (Markevitch 2010).
- Extended emission, which cannot be easily classified, was detected in A 1300 (the “candidate relic”, see Sect. 3.2.1). This source is arc–shaped and has a projected linear size of the order of ∼ 700 kpc and radio power $\log P_{325\ \mathrm{MHz}} = 6.9 \times 10^{24}$ WHz$^{-1}$ (assuming that it is at the cluster distance), and it is located at the periphery of the X–ray emission.
- A 1682 is the most enigmatic cluster in our study. Three filamentary features with no obvious optical counterpart are found: the N–W ridge, the E–tail and the S–E ridge. The latter is located at the boundary of the X–ray emission, but it is much smaller (at least in projection) than the typical size reported for relics, i.e. only ∼ 220 kpc, and has a radio power $\log P_{240\ \mathrm{MHz}} = 9.3 \times 10^{24}$ WHz$^{-1}$ if located at the distance of A 1682. The morphology, size and radio power of the N–W ridge argue in favour of a possible relic, but the direction of the steepening in the spectral index distribution is a puzzle. Our analysis of the E–tail disfavours the idea that it is related to the central double radio galaxy, even though at present there are no alternative explanations for its nature. Finally, diffuse very low surface brightness emission is visible south of the cluster centre, with total radio power $\log P_{240\ \mathrm{MHz}} = 6.8 \times 10^{24}$ WHz$^{-1}$ (assuming it is located at the distance of the hosting cluster). This radio emission could be the brightest part of an underlying more extended very low surface brightness radio halo.
- Our data suggest the presence of diffuse emission in A 781 just below the sensitivity threshold of the observations (Venturi et al. 2011a, see Table 5). This cluster deserves further investigation.

All the above results reinforce the overall finding that the diffuse cluster radio emission is more complex than the usual “radio halo” and “relic” classification when observed at frequencies of the order of ≤ 325 MHz.

### 4.4. Statistical correlations for radio halos at low frequency

The low frequency follow–up of the GMRT Radio Halo Cluster Survey has doubled the number of galaxy clusters with high sensitivity imaging of the radio halo at 325 MHz, bringing them to 14. We are aware that the statistics is still limited, but the numbers are significant enough to start investigating some correlations.

#### 4.4.1. Spectral index of radio halos and cluster temperature

Feretti et al. (2004), and more recently Giovannini et al. (2009), claimed a possible correlation between the cluster temperature and the radio halo spectral index, suggesting that hotter clusters host radio halos with flatter spectrum. If confirmed, this trend would provide important constraints on the origin of the emitting particles.

To investigate this point, to our new results we added all the remaining clusters in the literature with spectral information between 325 MHz and 1.4 GHz (A 2163, Coma, A 2255, A 665, A 2256 and A 754). Our analysis does not include A 209 and A 1300 (see Sect. 3.1.1 and 3.2.1 repsectively). Note that we used the updated values of $\alpha_{325\ \mathrm{MHz}}^{1.4\ GHz} = 1.65$ for A 697 (van Weeren et al. 2011) and $\alpha_{325\ \mathrm{MHz}}^{1.4\ GHz} = 1.3$ for A 2255 (Pizzo & de Bruyn 2009). These two values are considerably different than those used in the analysis of Giovannini et al. (2009), i.e. 1.2 and 1.7 respectively for A 679 and A 2255.
In the left panel of Fig. 10 we report the distribution of the clusters in the $\alpha_{325,1400}$–T plane. We do not find a clear correlation between these two quantities. Nevertheless, at a preliminary level our plot indicates that:

(1) clusters with T<10 keV host halos both with flat ($\alpha \sim 1$) and steep ($\alpha \sim 1.8$) spectrum;
(2) clusters with T>10 keV host halos with spectra flatter than $\alpha \sim 1.3$.

This behaviour is qualitatively consistent with the expectations of the re–acceleration models, which predict that

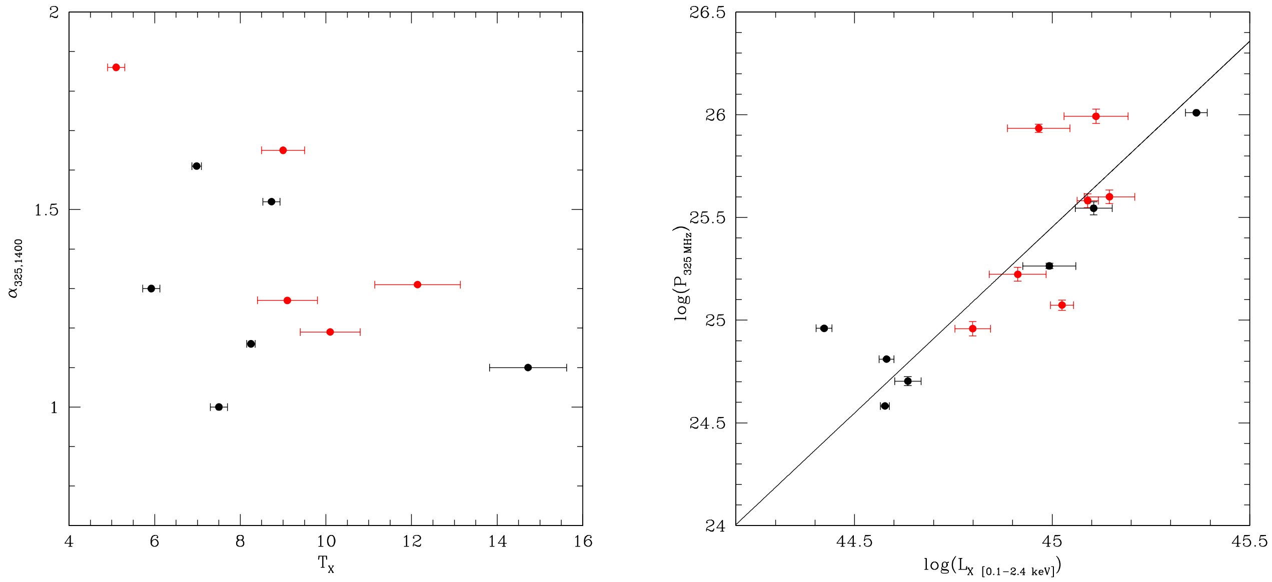

**Fig. 10.** *Left*: Spectral index of the radio halos presented in this paper and collected from the literature in the range 325 MHz–1.4 GHz plotted as function of the cluster X–ray temperature. *Right*: LogL$_{\rm X}$–LogP$_{325\ \rm MHz}$ correlation. The red points in each plot are the clusters from the GMRT 325 MHz follow-up.

radio halos have different spectra depending on the energy released into particle re–acceleration during mergers. In this case, from simple enery arguments, the fraction of halos with "flatter" spectra increases with the mass of the host cluster. In particular, if we restrict to the mass (temperature) range of our sample, moderately massive clusters (T$\sim 5 - 8$ keV) would statistically generate both "steep" and "flat" halos, while massive (T$>$ 8 keV) clusters would preferentially generate flatter halos (see Cassano et al. 2006 and Cassano et al. 2010). We are aware that information on more clusters is necessary to test any possible correlation between these two quantities.

### 4.4.2. LogL$_{\rm X}$–LogP$_{325\ \rm MHz}$ correlation

Beyond the GMRT clusters presented and discussed in this paper, we collected all the remaining clusters in the literature with high sensitivity imaging at 325 MHz ( A2163, Coma, A 2255, A 665, A 2256, A 754, A 2219) and derived the logL$_{\rm x}$–logP$_{325\ \rm MHz}$ correlation, which is shown in the right panel of Fig. 10. This analysis was presented in Kempner & Sarazin (2001) using WENSS data, and in Rudnick & Lemmerman (2009). For the first time we derive this correlation based on deep pointed observations with accurate subtraction of foreground and background sources projected onto the radio halo emission.

The best fit value of the slope is 1.81±0.28, consistent within the errors with what is found at 1.4 GHz, i.e. 2.06±0.20 (Brunetti et al. 2009).

Given the small size of the sample available at 325 MHz more data are needed to confirm the presence of the correlation and to constrain its slope. Cassano (2010) showed that in the framework of the turbulent re–acceleration scenario the correlation becomes steeper and broader at the LOFAR frequencies and sensitivities.

## 5. Conclusions

The GMRT Radio Halo Cluster Survey has been the first step towards the investigation of the statistical properties of radio halos in galaxy clusters. The most relevant results can be summarized as follows: (a) the bimodal distribution of galaxy clusters with respect to the presence of a radio halo (Brunetti et al. 2007) clearly shows that radio halos are not ubiquitous in clusters. The distribution of galaxy clusters in the logL$_{\rm X}$–logP$_{1.4\ \rm GHz}$ plot provides an important piece of information for the the theoretical models, suggesting that radio halos are transient radio sources (Brunetti et al. 2009, Enßlin et al 2011) [3]; (b) first quantitative correlations have been found between the dynamical state of clusters and the presence of halos, or lack thereof (Cassano et al. 2010). This result confirms that mergers play the most important role in the formation of radio halos; (c) a relevant byproduct of the survey was the discovery of ultra–steep spectrum radio halos. This poses new compelling constraints on the origin of these sources.

The results of the low frequency follow–up of radio halos and relics in the GMRT radio halo cluster sample reported in this paper, not only reinforce the radio halo/cluster merger connection, but also pose new important questions.

The study of the integrated synchrotron spectrum of the radio halos in our sample clearly shows a wide range of values for the spectral index, with $\Delta\alpha_{325\ \rm MHz}^{1.4\ \rm GHz} \sim 1.2 \div 1.9$, i.e. a difference of ∼1.4 in the power of the distribution of the radiating particles. This result, together with our points (a) and (b) above, is consistent with the expectations of the turbulent re–acceleration model, which makes the unique prediction of a high frequency break in the spectrum of the electrons emitting at radio frequencies. This reflects into a range of spectral slopes in the spectra of radio halos, including the ultra steep ones. At a more general level, these observational results suggest that inefficient mechanisms of particle acceleration activated during cluster mergers play an important role in the generation of radio halos.

---

[3] Using a SZ–selected sub–sample of the GMRT clusters, obtained from the first Planck cluster catalogue, Basu (2012) found that the cluster radio bimodality becomes considerably weaker in the Y$_{\rm ZS}$–logP plot, rising additional questions on the evolution of radio halos.

We found differences in the surface brightness distribution of the radio halos. Some of them are clumpy, others are centrally peaked and in other cases the isodensity contours are asymmetrically peaked. In some clusters we found a misplacement between the radio and X–ray peaks of emission, which deserves further investigation.

Bridges of emission, connecting (at least in projection) the relic and the radio halo emission were found in A 521, A 1300, A 2744 and RXCJ 1314.5–2515. Such features can be explained in the context of merger shocks and turbulence during merger processes (Markevitch 2010).

Our 325 MHz survey has doubled the number of clusters with high sensitivity imaging of the diffuse cluster scale emission at this frequency. This allowed us to start investigating some statistical properties of radio halos at low frequencies. For the first time we derived the correlation between the radio power at 325 MHz and the X–ray cluster luminosity by means of deep pointed observations. The slope is consistent within the errors with that derived at 1.4 GHz, however the correlation needs to be constrained on more solid basis with a larger number of data.

Finally, we investigated a possible trend between the radio halo spectral index and the temperature of the hosting cluster using the new data presented in the paper and updated information from the literature. With the data available at present, we cannot confirm the existence of the $\alpha$–T correlation claimed in Giovannini et al. (2009).

Our study shows that systematic high sensitivity low frequency imaging of diffuse cluster radio sources is the next step which needs to be taken to further improve our knowledge of the mechanisms at the origin of their formation.

*Acknowledgements.* We thank the staff of the GMRT for their help during the observations. GMRT is run by the National Centre for Radio Astrophysics of the Tata Institute of Fundamental Research. We acknowledge financial contribution from the Italian Ministry of University and Research, from MIUR grants PRIN2005 and 2006, from PRIN–INAF2005 and PRIN–INAF2008 and from contract ASI–INAF I/023/05/01. Support for S.G. was provided by NASA through Einstein Postdoctoral Fellowship Award Number PF0-110071 issued by the Chandra X-ray Observatory Center, which is operated by the Smithsonian Astrophysical Observatory.

## References

Bacchi, M., Feretti, L., Giovannini, G., et al., 2003, A&A, 400, 465
Basu, K., 2012, MNRAS Letters, 421L, 112
Blasi, P., Colafrancesco, S., 1999, A. Ph., 12, 1999
Böhringer, H., Schuecker, P., Guzzo, L., et al., 2004, A&A, 425, 367
Bonafede, A., Feretti, L., Giovannini, G., et al., 2009, A&A, 503, 707
Bondi, M., Ciliegi, P., Venturi, T., et al., 2007, A&A, 463, 519
Boschin, W., Girardi, M., Barrena, R., et al., 2012, A&A, 340A, 143
Bourdin, H., Mazzotta, P., Markevitch, M., et al., 2012, submitted to ApJ
Brown, S., Rudnick, L., 2011, MNRAS, 412, 2
Brunetti, G., Setti, G., Feretti, L., Giovannini, G., 2001, MNRAS, 320, 365
Brunetti, G., & Blasi, P., 2005, MNRAS, 363, 1173
Brunetti, G., Venturi, T., Dallacasa, D., et al., 2007, ApJ, 670, L5
Brunetti, G., Giacintucci, S., Cassano, R., et al., 2008, Nature, 455, 944
Brunetti, G., Cassano, R., Dolag, K., et al., 2009, A&A, 507, 661
Brunetti, G., & Lazarian, 2012, MNRAS, 412, 817
Brunetti, G., 2011, in *Non–thermal phenomena in colliding galaxy clusters*, Mem. SAIT, 82, 515
Buote, D.A., 2001, ApJ 553, 15
Carretti, E., Brown, S., Stavaley–Smith, L., et al., 2012, MNRAS, in press (arXiv:1205.1082v1)
Cassano, R., 2009, in *The low frequency radio Universe*, Eds. D. J. Saikia, D. A. Green, Y. Gupta and T. Venturi, ASP Conf. Ser. 407, 223
Cassano, R., Brunetti, G., 2005, MNRAS, 357, 1313
Cassano, R., Brunetti, G., Setti, G., 2006, MNRAS, 369, 1577
Cassano, R., Brunetti, G., Venturi, T., et al., 2008, A&A, 480, 687
Cassano, R., 2010, A&A, 517A, 10
Cassano, R., Ettori, S., Giacintucci, S., et al., 2010, ApJ Letters, 721, L82
Cassano, R., Brunetti, G., Venturi, T., 2011, Journal of Astroph. Astron., 32, 519
Clarke, T. E., & Enßlin, T. A., 2006, AJ, 131, 2900
Dallacasa, D., Brunetti, G., Giacintucci, S., et al., 2009, ApJ, 699, 1288
David, L.P., Kempner, J., 2004, ApJ, 613, 840
Dennison, B., 1980, ApJ Letters, 239, L93
Dwarakanath, K.S., Rudnick, L., Shankar, N.U., Venturi, T., 2011, *Diffuse Relativistic Plasmas*, Bangalore, 1–4 March 2010, Conference Proceedings, Published by Indian Academy of Sciences, Journal of Astroph Astron., Vol. 32, N. 4
Enßlin, T.A., Bierman, P.L., Klein, U., et al., 1998, A&A, 332 395
Enßlin, T., Gopal–Krishna, 2001, A&A, 366, 26
Enßlin, T., Pfrommer, C., Miniati, F., et al., 2011, A&A, 527A, 99
Feretti, L., Brunetti, G., Giovannini, G., et al., 2004, JKAS, 37,315
Feretti L., Schuecker, P., Böringer, H., et al., 2005, A&A, 444, 157
Feretti, L., Giovannini, G., Govoni, L., et al., 2012, The Astronomy & Astrophysics Review, 20, 54
Ferrari, C., Govoni, F., Schindler, S., et al., 2008, SSRv, 134, 93
Ferrari, C., Brüggen, M., Brunetti, G., Venturi, T., 2011, *Non–thermal phenomena in colliding galaxy clusters*, Nice 15–18 November 2010, Conference Proceedings, Editor F. Serra, MemSAIt, Vol. 82, N. 3
Finoguenov, A., Sarazin, C. L., Nakazawa K., et al., 2010, ApJ, 715, 1143
Fujita, Y., Takizawa, M., & Sarazin, C.L., 2003, ApJ, 584, 190
Geller, M.J., Dell'Antonio, I.P., Kurtz, M.J., et al., 2005, ApJ, 635L, 125
Giacintucci, S., Venturi, T., Macario, G., et al., 2008, A&A, 486, 347
Giacintucci, S., Venturi, T., Brunetti, G., et al., 2009, A&A, 505, 45
Giacintucci, S., Cassano, R., Brunetti, G., et al., 2013, to be submitted to ApJ (G12)
Giovannini, G., Bonafede, A., Feretti, L., et al., 2010, A&A, 507, 1257
Girardi, M., Mezzetti, M., 2001, ApJ, 548, 79
Govoni, F., Feretti, L., Giovannini G., et al., 2001, A&A, 376, 803
Govoni, F., Markevitch, M., Vikhlinin A., et al., 2004, ApJ, 605, 695
Govoni, F., Murgia, M., Giovannini, G., et al., 2011, A&A, 529A, 69
Hao, J., McKay, T.A., Koester, B. et al., 2010, ApJS, 191, 254
Hoeft, M., Brüggen, M., 2007, MNRAS, 375, 77
Jaffe, W.J., 1977, ApJ, 216,212
Kempner, J.C., Sarazin, C.L., 2001, ApJ, 548, 639
Kempner, J.C., David, L.P., 2004, MNRAS, 385, 392
Keshet, U., & Loeb, A., 2010, ApJ, 722, 737
Kim, K.-T., Kronberg, P.P., Giovannini, G., et al., 1989, Nature, 341, 720
Koester, B.P., McKay, T.A., Annis, J., et al. 2007, ApJ, 660, 239
Lemonon, L., Pierre, M., Hunstead, R.W., et al., 1997, A&A, 326, 34
Liang, H., Hunstead, R.W., Birkinshaw, M., et al., 2000, ApJ, 544, 686
Macario, G., Venturi, T., Brunetti, G., et al., 2010, A&A, 517, A43
Macario, G., Markevitch, M., Giacintucci, S., et al., 2011a, ApJ, 728, 82
Macario, G., Venturi. T., Dallacasa D., et al., 2011b, in *Non–thermal phenomena in colliding galaxy clusters*, Mem. SAIT, 82, 557
Macario, G., Venturi, T., Intema, H., et al., 2012, submitted to A&A
Markevitch, M., Gonzalez, A. H., David, L., et al., 2002, ApJ, 567, 27
Markevitch, M., Govoni, F., Brunetti, G., et al., 2005, ApJ, 627, 733
Markevitch, M., 2010, 12th Marcel Grossman Meeting, Paris, arXiv:1010.3660v1

Mazzotta, P., Bourdin, H., Giacintucci, S., et al., 2011, in *Non–thermal phenomena in colliding galaxy clusters*, Mem. SAIt, 82, 495

Merten, J., Coe, D., Dupke, R., et al., 2011, MNRAS, 417, 333

Morrison, G.E., **et al.**, 2003, ApJSS, 146, 267

O'Dea, C.P., Owen, F.N., 1985, AJ, 90, 954

O'Dea, C.P., Sarazin, C.L., Owen, F.N., 1877, ApJ, 316, 113

Ogrean, G., Brüggen, M., Röttgering, H., et al., 2012, submitted to MNRAS (arXiv:1201.1502O)

Orrú, E., Murgia, M., Feretti, L., et al., 2007, A&A, 467, 943

Owers, M. S., Couch, W.J., Nulsen, P.E.J., et al., 2012, ApJ, 750L, 23

Petrosian, V., 2001, ApJ, 577, 560

Pfrommer, C., Enßlin, T.A., 2004, JKAS, 37, 455

Pierre, M., Oukbir, J., Dubreuil, D., et al., 1997, A&AS, 124, 283

Pizzo, R., de Bruyn, A.G., 2009, A&A, 507, 639

Ragozzine, B., Clowe, D., Markevicth, M., et al., 2012, ApJ, 744, 94

Reid, A.D., Hunstead, R.W., Lemonon, L., et al., 1999, MNRAS, 302,571 (R99)

Roland, J., 1981, A&A, 93, 407

Rudnick, L., Lemmerman, J.A., 2009, ApJ, 697, 1341

schlickeiser, R., Sievers, A., Thiemann, H., 1987, A&A, 182, 21

Valtchanov, I., Murphy, T., Pierre, M., et al., 2002, A&A, 392, 795

van Weeren, R.J., Röttgering, H.J. A., Brüggen, M., Hoeft, M., 2010, Science, 330, 347

van Weeren, R.J., Brüggen, M., Röttgering, H.J.A., et al., 2011, A&A, 533, A35

van Weeren, R., Intema, H.T., Röttgering, H.J.A., et al., 2011b, in *Non–thermal phenomena in colliding galaxy clusters*, MemSAIt, 75, 282

van Weeren, R.J., Bonafede, A., Ebeling, H., et al., 2012, MNRAS, in press (arXiv:1206.2294)

Venturi, T., Bardelli, S., Zagaria, M., et al., 2002, A&A, 385, 39

Venturi, T., Giacintucci, S., Brunetti, G., et al., 2007, A&A, 463, 937 (V07)

Venturi, T., Giacintucci, S., Dallacasa, D., et al., 2008, A&A, 484, 327 (V08)

Venturi, T., 2011, in *Non–thermal phenomena in colliding galaxy clusters*, Mem. SAIT, 82, 499

Venturi, T., Giacintucci, S., Dallacasa, D., et al., 2011a, MNRAS Letters, 414, L65

Venturi, T., Giacintucci, S., Dallacasa, D., 2011b, Journal of Astroph. and Astron., 32, 501

Ziparo, F., Braglia, F.G., Pierini, D., et al., 2012, MNRAS, 420, 2480

**Table 1.** Clusters observed with the GMRT

| Cluster name | RA (h m s) | DEC (° ′ ″) | z | Radio Source | Ref. | scale (kpc/″) |
|---|---|---|---|---|---|---|
| A 2744 | 00 14 18.8 | −30 23 00 | 0.307 | GRH | a | 4.526 |
| A 209 | 01 31 53.0 | −13 36 34 | 0.206 | GRH | a | 3.377 |
| A 521 | 04 54 09.1 | −10 14 19 | 0.248 | GRH+Rel | b, c, d | 3.887 |
| A 697 | 08 42 53.3 | +36 20 12 | 0.282 | GRH | e | 4.265 |
| A 781 | 09 20 23.2 | +30 26 15 | 0.298 | Rel+Candidate RH | f | 4.434 |
| Z 2661 | 09 49 57.0 | +17 08 58 | 0.383 | Candidate RH | a | 5.231 |
| A 1300 | 11 31 56.3 | −19 55 37 | 0.308 | RH+Rel | a | 4.536 |
| A 1682 | 13 06 49.7 | +46 32 59 | 0.226 | Candidate RH+Rel | a, g | 3.626 |
| RXCJ 1314.4–2515 | 13 14 28.0 | −25 15 41 | 0.244 | RH+Double Rel | a, h | 3.840 |
| A 1758N | 13 32 32.1 | +50 30 37 | 0.280 | RH | a | 4.244 |
| RXCJ 2003.5–2323 | 20 03 30.4 | −23 23 05 | 0.317 | GRH | i | 4.625 |

Notes: a: This paper; b: Giacintucci et al. 2008; c: Brunetti et al. 2008; d: Dallacasa et al. 2009; e: Macario et al. 2010; f: Venturi et al. 2011a; g: Venturi et al. 2011b; h: Mazzotta et al. 2011; i: Giacintucci et al. 2009.

**Table 2.** Details of the GMRT observations presented in this paper.

| Cluster name | $\nu$ (MHz) | $\Delta\nu$ (MHz) | Obs. time (hr) | HPBW, PA $^a$ (″×″, °) | rms (mJy b$^{-1}$) |
|---|---|---|---|---|---|
| A 2744 | 325 | 32 | 8 | 15.9×8.5, 38 | 0.15 |
| A 209 | 325 | 32 $^b$ | 8 | 11.0×8.7, 30 | 0.12 |
| Z 2661 | 325 | 32 | 10 | 10.8×8.4, −83 | 0.12 |
| A 1300 | 325 | 32 $^b$ | 8 | 14.0×8.8, 8 | 0.45 |
| A 1682 | 240 | 8 | 6 | 13.4×10.1, 47 | 0.58 |
| RXCJ 1314.4–2515 | 325 | 32 | 8 | 15.1×8.0, 32 | 0.16 |
| A 1758N | 325 | 32 | 8 | 10.5×8.4, 58 | 0.10 |

Notes: *a*: Half-power beamwidth and position angle of the full array; *b*: the observations were carried out using a total bandwidth of 32 MHz (USB+LSB), but only the USB was used for the analysis.

**Table 3.** Properties of the discrete radio sources

| Cluster name | Source | RA [a] (h,m,s) | DEC [a] ($^{\deg}$,′,″) | $S_{\rm peak,325MHz}$ (mJy beam$^{-1}$) | $S_{\rm tot,325MHz}$ (mJy) |
|---|---|---|---|---|---|
| A 2744 | S1 | 00 14 21.6 | −30 25 56 | 7.4 | 14.0 |
| | S2 | 00 14 33.8 | −30 22 31 | 6.3 | 7.5 |
| | S3 | 00 14 39.9 | −30 28 20 | 2.1 | 2.4 |
| | S4 | 00 14 44.5 | −30 26 20 | 9.8 [b] | 83.6 [b] |
| A 209 | S1 | 01 31 52.5 | −13 37 00 | 40.9 [b] | 81.7±4.1 [b] |
| | S2 | 01 31 56.5 | −13 35 17 | 7.0 | 13.2±0.7 |
| Z 2661 | S1 | 09 49 47.1 | +17 06 00 | 2.0 [b] | 7.8 [b] |
| | S2 | 09 49 49.1 | +17 06 57 | 3.0 | 5.1 |
| | S3 | 09 49 50.3 | 17 06 34 | 1.5 [b] | 3.2 [b] |
| | S4 | 09 49 52.5 | 17 07 34 | 6.2 | 8.7 |
| A 1300 | A1 | 11 31 54.4 | −19 55 39 | 50.3 | 60.8 |
| | A2 | 11 31 54.3 | −19 53 55 | 92.5 [b] | 197.8 (216.1) [b,c] |
| | A3 | 11 31 54.9 | −19 52 05 | 14.1 [b] | 23.1 [b] |
| | B1 | 11 31 43.7 | −19 52 55 | 19.6 [b] | 40.7 [b] |
| A 1682 | S1 | 13 06 45.6 | +46 33 32 | 400.0 [b] | 1131.6 [b,d] |
| | S2 | 13 06 49.9 | +46 33 33 | 29.8 | 50.3 |
| | S3 | 13 07 03.7 | +46 33 47 | 5.6 | 6.9 |
| RXCJ 1314.4–2515 | S1 | 13 14 30.4 | -25 17 15 | 5.8 | 11.5 |
| | S2 | 13 14 48.5 | -25 16 17 | 7.9 | 18.0 |
| A 1758N | S1 | 13 32 35.7 | +50 32 35 | 1.0 | 2.0 |
| | S2 | 13 32 39.0 | +50 33 36 | 16.9 | 21.0 |
| | S3 | 13 32 39.9 | +50 34 32 | 18.8 | 27.2 |
| | S4[a] | 13 32 54.8 | +50 31 35 | 145.3 [b] | 514.6 |
| | S5 | 13 32 59.6 | +50 31 22 | 18.0 | 40.34 |

Notes: *a*: coordinates of the radio peak; *b*: measured using TVSTAT; *c*: the value in brackets includes the *bridge* between A1 and A2; *d*: this value includes the E tail.

**Table 4.** Properties of the diffuse cluster sources in the GMRT Radio Halo Survey

| Cluster name | Radio source | $\nu$ (MHz) | $S_\nu$ (mJy) | $P_\nu$ W HZ$^{-1}$ | LLS (Mpc) | HPBW (″×″) |
|---|---|---|---|---|---|---|
| A 2744 | GRH | 325 | 323±26 | $9.68\times10^{25}$ | ∼1.9 | 35.0×35.0 |
| | Rel | 325 | 122±10 | $3.66\times10^{25}$ | ∼1.3 | 35.0×35.0 |
| A 209 | GRH | 325 | 74±6[a] | $8.91\times10^{24}$ | ∼ 0.6[a] | 25.0×25.0 |
| A 1300 | GRH | 325 | 130±10 | $3.92\times10^{25}$ | ∼0.9 | 28.0×28.0 |
| | Rel | 325 | 75±6 | $2.26\times10^{25}$ | ∼0.5 | 28.0×28.0 |
| | Cand. Rel | 325 | 23±2 | $6.94\times10^{24}$ | ∼0.7 | 28.0×28.0 |
| A 1682 | Diffuse Comp. | 240 | 46±4 | $6.82\times10^{24}$ | ∼0.3 | 18.3×14.0 |
| RXCJ 1314.4–2515 | W Rel | 325 | 137±11 | $2.42\times10^{25}$ | | 26.1×10.2 |
| | E Rel | 325 | 52±4 | $9.18\times10^{24}$ | | 26.1×10.2 |
| | RH | 325 | 40±3 | $7.06\times10^{24}$ | | 26.1×10.2 |
| A 1758N | GRH | 325 | 155±12 | $3.75\times10^{25}$ | ∼1.5 | 35.0×35.0 |
| A 521[b] | GRH | 240 | 152±15 | $2.79\times10^{25}$ | ∼0.9 | 35.0×35.0 |
| A 521[b] | Rel | 240 | 180±10 | $3.30\times10^{25}$ | ∼1 | 35.0×35.0 |
| A 521[c] | Rel | 325 | 114±6 | $2.09\times10^{25}$ | ∼1 | 16.0×13.0 |
| A 697[d] | GRH | 325 | 47.3±2.7 | $1.16\times10^{25}$ | ∼1.3 | 46.8×41.4 |
| A 781[e] | Rel | 325 | 93.3±7.5 | $2.61\times10^{25}$ | ∼0.8 | 40.0×37.0 |
| RXCJ 2003.5–2323[f] | GRH | 240 | 360±18 | $1.16\times10^{26}$ | ∼1.4 | 35.0×35.0 |

Notes: [a]: The value should be considered a lower limit, see Section 3.1.1. [b] Information taken from Brunetti et al. 2008 [c] Information taken from Giacintucci et al. 2008. [d] Information taken from Macario et al. 2010. [e] Information taken from Venturi et al. 2011a. [f] Information taken from Giacintucci et al. 2009.

**Table 5.** Candidate diffuse cluster emission

| Cluster name | Candidate source | $\nu$ (MHz) | $S_\nu$ (mJy) |
|---|---|---|---|
| A 781[a] | USSRH? | 325 | ∼20-30 |
| A 1682[b] | GRH? | 240 | ∼ 80 |
| Z 2661[c] | RH? | 610 | ∼5.9 |

Notes: [a]: From Venturi et al. 2011a. [b]: From Venturi et al. 2011b. [c]: From V08.